Seismic and Infrasound Signals at Mt. Etna: Modelling the North-East Crater Conduit and its Relation with the 2008-2009 Eruption Feeding System

Mariangela Sciotto
Dipartimento di Scienze Biologiche, Geologiche e Ambientali, Sezione Scienze della Terra, Università di Catania, Corso Italia 57, 95129 Catania, Italy

Andrea Cannata
Istituto Nazionale di Geofisica e Vulcanologia, Osservatorio Etneo, Sezione di Catania, Piazza Roma 2, 95123 Catania, Italy

Stefano Gresta
Dipartimento di Scienze Biologiche, Geologiche e Ambientali, Sezione Scienze della Terra, Università di Catania, Corso Italia 57, 95129 Catania, Italy
Istituto Nazionale di Geofisica e Vulcanologia, Via di Vigna Murata 605,00143 Roma, Italy

Eugenio Privitera*
Istituto Nazionale di Geofisica e Vulcanologia, Osservatorio Etneo, Sezione di Catania, Piazza Roma 2, 95123 Catania, Italy

Laura Spina
Dipartimento di Scienze Biologiche, Geologiche e Ambientali, Sezione Scienze della Terra, Università di Catania, Corso Italia 57, 95129 Catania, Italy
Department of Earth and Environmental Sciences, Section for Mineralogy, Petrology and Geochemistry, Theresienstr. 41, 80333 Munich, Germany

***Corresponding author**

Telephone number: +39 095 7165800
Fax number: +39 095 7165826
E-mail address: eugenio.privitera@ct.ingv.it

Abstract

On 13 May 2008, an eruption began at Mt. Etna from an eruptive fissure that opened on the upper eastern flank of the volcano. During 12-13 May, 157 infrasonic events, together with the related seismic transients, were collected. We carried out several analyses to obtain dominant frequencies, pseudospectrograms, peak-to-peak amplitudes, source locations and time lags between infrasonic and seismic events. Spectra of the infrasonic events show two main spectral peaks in the frequency bands ~0.4-0.7 Hz and 1.5-2.0 Hz, respectively. Both infrasonic and seismic events were separately located below the North-East Crater, where no eruptive activity was observed. Moreover, significant changes in infrasound spectral content, as well as in the infrasonic-seismic lags, were found a few hours before the beginning of the eruption. On the basis of the collected information the infrasound source mechanism was modelled as a superposition of pipe and Helmholtz resonance, also leading to outline the geometry of the shallower portion of the North-East Crater plumbing system. The occurrence of these seismo-infrasonic events together with other geological and geophysical evidences, led us to inferring a direct link between North-East Crater activity and the eruptive fissure. Further, based on variations over time of both spectral features and seismic-infrasonic time lag, shallowing phenomena of the free magma column inside North-East Crater conduit were hypothesized. Such an uprise of magma was likely caused by a pressure increase inside the plumbing system occurring before the beginning of the 2008-2009 eruption.

Keywords: infrasound, Helmholtz resonator, plumbing system geometry, seismo-acoustic studies, Mt. Etna

Highlights:

- Seismo-acoustic studies were performed on the few hours before the 2008-2009 eruption.
- Seismo-infrasonic events from NE crater preceded the 2008-2009 fissure eruption.

- Seismo-infrasonic events allowed modelling the shallower portion of NEC plumbing system.
- Superposition of pipe and Helmholtz resonance phenomena was hypothesized.
- Spectral and seismic-infrasonic lag changes suggest magma shallowing inside NEC conduit.

1. Introduction

Over the last decade, the analysis of infrasound signals has become a valuable tool in volcanic activity monitoring, since many phenomena acting in volcanic areas generate infrasonic waves (for instance explosive activity, pyroclastic flow, rockfall and degassing). One of the advantages of infrasonic wave studies lies in the Green's function, which at local distances (< 10 km) are less affected by propagation effects with respect to the seismic ones (Arrowsmith et al., 2010). Further, infrasound travels for long distances and can therefore be recorded at remote sensors (Fee et al., 2010a).

In recent years, infrasound observations in volcanic areas have demonstrated their usefulness in the investigations on explosive and degassing phenomena (e.g. Vergniolle and Ripepe, 2008; Cannata et al., 2009a,b; Matoza et al., 2009; Fee et al., 2010b). Such studies have provided new insights into eruption source mechanisms, on constraining the source position and obtaining quantitative information on the plume features (velocity, height and eruptive flux) (e.g. Petersen and McNutt, 2007; Caplan-Auerbach et al., 2009). In addition, by analysing infrasonic signals, inferences on the geometry of the very shallow part of plumbing systems have been made (e.g. Fee et al., 2010b; Goto and Johnson, 2011).

Infrasound monitoring in volcanic areas has also been widely used in multi-disciplinary studies (e.g. Sahetapy-Engel et al., 2008; Pistolesi et al., 2011; Sciotto et al., 2011). In particular, it has proved to be very useful in conjunction with seismic signal analysis (Arrowsmith et al., 2010). Such studies allow a better understanding of eruptive dynamics since they separate shallow or subaerial processes from deeper phenomena (Zobin, 2012), and have proved fundamental to constrain the

explosive source depth (Kobayashi et al., 2005; Petersen and McNutt, 2007), to investigate the eruption style (Johnson and Aster, 2005) as well as the acoustic properties of the fluid-filled conduit (Hagerty et al., 2000).

Seismo-acoustic studies have also been recently performed at Mt. Etna (e.g. Di Grazia et al., 2009; Sciotto et al., 2011). Currently, Etna is characterized by four active summit craters: Voragine, Bocca Nuova, South-East Crater and North-East Crater (hereafter referred to as VOR, BN, SEC and NEC, respectively; **Fig. 1**). Infrasound radiation from these vents can be classified into continuous and sporadic activity. The former consists in short-duration releases of pressure bursts constantly generated by NEC and related to degassing activity (Cannata et al., 2009b), while the latter occurs solely during explosive activity (Strombolian explosions, lava fountains, ash emissions). Indeed, over the last few years, SEC and BN have generated infrasonic tremor and amplitude transients during eruptive episodes (e.g. Cannata et al., 2011).

In this work, we will focus on the analyses of seismo-acoustic events recorded during 12-13 May 2008, just before the onset of the 2008-2009 flank eruption. Many authors have already studied this eruption, investigating the evolution of activity and magma ascent dynamics through ground deformation, magnetic variations, as well as infrasonic and seismic data (Napoli et al., 2008; Aloisi et al., 2009; Cannata et al., 2009a; Di Grazia et al., 2009; Bonaccorso et al., 2011; Langer et al., 2011).

The aim of the work is to track the changes in the characteristics of seismo-acoustic events (occurring on 12 and 13 May) and to examine the links to the impending eruption. Further, infrasound source mechanism will also be investigated to acquire new insights into the shallower portion of the Mt. Etna plumbing system.

2. Volcanic framework

On 13 May 2008, a new eruption began at Mt. Etna with the opening of a system of eruptive fissures in the upper eastern flank of the volcano. Since January 2007, an inflation pattern had been

recorded by the local GPS network (Aiuppa et al., 2010; Bonaccorso et al., 2011), suggesting a magma recharge phase. Volcanic activity during 2007 was marked by 6 paroxysmal episodes (Langer et al., 2011), among which two (29 April and 6-7 May) were characterized by Strombolian activity at the summit of SEC, whereas the other four exhibited sustained lava fountaining, respectively located at SEC (29 March and 10-11 April) and at a vent in the lower E slope of the cone (4-5 September and 23-24 November). All the explosive events had variable duration and were accompanied by lava effusion (Langer et al., 2011). From January 2008, more evident extensions of GPS baselines, located at relatively low altitude, and the occurrence of deep earthquakes were further evidence of the volcanic system recharging (Di Grazia et al., 2009). About two months before the eruption onset there was significant deformation also at higher altitude. The seismicity increased and was located on the NE, E and S flanks of the volcano. Furthermore, a violent explosive eruption started at about 14:00 on 10 May 2008 (all times are GMT) and was preceded and accompanied by an increase in volcanic tremor amplitude (Patanè et al., 2011). Strombolian activity took place at the vent in the lower E flank of the cone and was rapidly replaced by a lava fountain. This paroxysmal episode ceased at about 18:00 on the same day and preceded by three days the beginning of the 2008-2009 flank eruption. At 08:39 on 13 May, the occurrence of a seismic swarm, located NE of the summit craters between -1.5 and 1.5 km a.s.l. (Cannata et al., 2009a), together with significant ground deformation (Aloisi et al., 2009), heralded the ascent of magma in the shallower portion of the volcano and the impending eruption. The magma intrusion caused, at about 09:30, the opening of a N140°E eruptive fissure extending between 3050 and 2950 m a.s.l. and fed both a lava fountain from its northern part and lava flows (Bonaccorso et al., 2011; Cannata et al., 2011). Successively, the fissure propagated downslope to ~2650 m a.s.l. in south-eastward direction (see EF in the inset of **Fig. 1**), where Strombolian activity and lava effusion took place (Bonaccorso et al., 2011). A few hours later, an asymmetric graben (2300 m long) formed north of NEC, with NNW-SSE and N-S dry fractures (Bonaccorso et al., 2011; **Fig. 1**). The eruption continued until July 2008, with alternating periods of decreasing and renewed Strombolian

activity and lava effusion (Cannata et al., 2011). Then, the eruption was mainly effusive and continued until 6 July 2009.

3. Data acquisition

We used data from 6 seismic stations located between 1500 and 3000 m a.s.l. and 4 infrasonic stations sited around summit craters with altitude in the range ~2800-3000 m a.s.l. (**Fig. 1**). The stations, belonging to the permanent seismic and infrasonic networks, are run by Istituto Nazionale di Geofisica e Vulcanologia, Osservatorio Etneo - Sezione di Catania. Seismic stations are equipped with broadband (40 s cut-off period), 3-component Trillium seismometers (Nanometrics™) and infrasonic stations are equipped with Monacor condenser microphone with a sensitivity of 80 mV/Pa in the 1-20 Hz infrasound band. Seismic and infrasound signals were acquired at a sampling rate of 100 Hz.

Since Monacor microphones do not have flat response in the whole frequency range of interest, (generally 0.3-6 Hz), laboratory tests were performed on recording ambient noise with both a Monacor and a G.R.A.S. 40AN microphone. The G.R.A.S. 40AN sensor shows a flat response with sensitivity of 50 mV/Pa in the frequency range 0.3-20,000 Hz, and ±3 dB in the range 0.1-0.3 Hz. Thus, on the basis of the response of G.R.A.S. sensor the "experimental" response curve of the Monacor microphone was calculated to correct the amplitude values, spectra and pseudospectrograms (reported further on).

4. Data analysis

To carefully investigate the volcano dynamics just a few hours before the beginning of the eruption, seismic and infrasound signals, recorded during 12-13 May 2008, were studied.

From the deployment of the permanent infrasonic network and until 12 May 2008, during a non-eruptive period, infrasound activity consisted of amplitude transients with dominant frequency

between 1 and 2.5 Hz, recorded almost continuously and related to the degassing activity of NEC (Spina et al., 2011).

The amplitude of infrasound signal recorded on 12 and 13 May (**Fig. 2a**) and the related RMS values gradually increased from ~20:00 on 12 May, until the onset of the eruption (9:30 on 13 May, **Fig. 2b**) when they sharply reached the maximum value.

The infrasonic events were extracted by applying the STA/LTA trigger algorithm (Withers et al., 1998) on the signal recorded at EBEL (**Fig. 1**), the reference station in this study, since less affected by noise. On the basis of the infrasonic event features, we fixed the short and the long window of trigger algorithm equal to 0.6 s and 6 s, respectively, and filtered the signal in the frequency band 0.2-2 Hz, thus detecting 157 events. We evaluated the time evolution of the occurrence rate (**Fig. 2c**) by counting the number of infrasonic events in a 30-minute-long window. The occurrence rate showed a maximum around 22:00 on 12 May (13 events per 30 minutes), whereas it underwent a slight decrease in the hours preceding the onset of the eruption, partly due to the higher background signal level. Such infrasonic events lasted 10-15 s and were characterized by an impulsive and powerful first pulse followed by decaying sinusoidal oscillations (**Fig. 3**).

We analyzed such events in the frequency domain, and visualized the time evolution of the spectral content by means of the pseudospectrogram (**Fig. 4a**). It is made up of 48 spectra, each of which was obtained averaging the spectra (calculated by applying FFT on roughly 5-s-long windows) of the events occurring during 1-hour-long time spans. The white areas in the pseudospectrogram represent time spans with almost no events or none at all. Indeed, in order to be drawn, each column of the pseudospectrogram needs at least one event occurring in each of the two contiguous 1-hour-long windows. The pseudospectrogram highlighted how the infrasonic events radiated energy mostly in the frequency band 0.4-2.5 Hz. In particular, two spectral peaks were dominant in the frequency bands 0.4-0.7 and 1.5-2.0 Hz. The main temporal variations are the frequency increase of the higher spectral peak and the coincident appearance of the lower frequency peak roughly at

16:00 on 12 May. A slight frequency increase of the lower spectral peak occurred a few hours before the onset of the eruption.

To better investigate these two frequency bands and their temporal variations, by using a 10s-long signal window we calculated the dominant peak frequencies separately in two frequency bands: 0.2-1 and 1-5 Hz. Analysing the higher band, we noticed that the peak frequency gradually increased from 1.5 to about 2.0 Hz during 12 May, while on 13 May it remained fairly steady until the onset of the eruption (**Fig. 4b**). The lower band exhibited an increase in the peak frequency from 0.4 to 0.7 Hz from 00:00 on 13 May to the onset of the eruption (**Fig. 4c**). Moreover, for the infrasonic event characterization we estimated the peak-to-peak amplitudes in both the spectral bands. From 13 May the peak-to-peak amplitudes showed a gradually increasing trend, which was more pronounced for the lower frequency band (**Fig. 4d, e**).

While in most cases NEC events lacked any seismic counterpart or were accompanied by very weak seismic signals (Spina et al., 2011), clear long-period seismic events are associated with the NEC events preceding the eruption (**Fig. 3**). It is noteworthy that a few infrasonic events with the associated seismic events had also been recorded in the hours preceding the lava fountain on 10 May 2008. They exhibited similar frequency content but lower peak-to-peak amplitudes.

Figure 5a, b shows an example of an infrasonic event of 13 May with the coupled seismic one (raw traces). Both the events exhibit similar spectral content, especially at low frequency (< 1 Hz; **Fig. 5c, d**).

All the four stations were used to locate the infrasonic event source by applying a composite method based on semblance and brightness functions. The method is based on a grid search over a 6x6 km^2 surface with spacing between nodes of 50 m. The source was located in the grid node with the largest composite semblance-brightness value (for details see Cannata et al., 2011 and references therein). **Figures 6a, b** and **7a** show how the locations are well-aligned along the NEC coordinates (red dotted lines in **Fig. 6**) for the whole period. Moreover, we located the seismic events associated with the infrasonic ones. We performed the location analysis by using a grid

search method based on the joint computation of two different functions: semblance function and R^2, the latter parameter is calculated on the basis of the spatial distribution of seismic amplitudes. The grid was 6x6x4 km^3 with spacing of 250 m. Also in this case, the source was located in the node with the largest composite semblance-R^2 value (for details see Patanè et al., 2011 and reference therein). 54 seismic events were located (see **Figures 6c-e** and **7b**). Similarly to the infrasonic events, the seismic events are roughly located below NEC and did not exhibit significant time variations. It is also evident how the seismic locations are more scattered than the infrasonic ones (**Fig. 6**). The higher precision and accuracy of the infrasonic locations is due to the simpler velocity structure of the atmosphere (which can generally be considered homogeneous for short propagation distances, e.g. within 5 km of the vent) compared to the volcano edifice velocity structure (Johnson, 2005). This is also owing to the lower velocity of infrasonic waves, with respect to the seismic ones. Indeed, in both the location algorithms (semblance-brightness and semblance-R^2 for infrasound and LP events, respectively) the size of the area/volume with high values of semblance-brightness or semblance-R^2 depends heavily on the velocity: the higher the velocity, the wider the area/volume, and hence less precise the source location. This is also clearly evidenced in **Figure 8**, showing the space distribution of semblance-brightness and semblance-R^2 of the infrasound and seismic components, respectively, of a selected seismo-infrasonic event. Unlike the semblance-brightness distribution, exhibiting a very narrow area with high values, the semblance-R^2 distribution highlights a much larger high-value volume, and then a less resolved source location.

The comparison between the seismic and infrasonic traces (filtered in the band 0.2-1 Hz) in **Figure 5e** highlights the similarity of their waveforms and their time lag. On the basis of the seismic-infrasonic lag several authors estimated the source depth (e.g. Ripepe and Braun, 1994; Ripepe et al., 2001a; Gresta et al., 2004; Petersen and McNutt, 2007). Small variations of the lag can give information about the changes in source location and propagation medium properties (e.g. Kobayashi et al., 2005). To this end, we evaluated the temporal evolution of the lag at station

EBEL. In order to make the results of this analysis more robust we used the cross-correlation function. Once the window containing the infrasonic event is selected, the cross-correlation analysis tracks down the seismic window including the similar seismic event. Thus, the lag is calculated between the windows which showed the maximum cross-correlation coefficient (a similar method was used by Ripepe et al., 2001b). We chose 4-second-long windows, a window shift step of 0.05 s and a cross-correlation coefficient threshold of 0.7. The results are shown in **Figure 9** (orange dots). Following this procedure we were able to calculate the lag only for ~30 events of the whole dataset due to the high level of volcanic tremor affecting the seismic recordings. To overcome this drawback, we also measured the lag by means of an accurate manual procedure. By picking the onset of infrasonic and seismic events, we found the lag values shown in **Figure 9** (blue dots). The results obtained by the two procedures were comparable and highlighted a decreasing trend in the lag a few hours preceding the eruption. In particular, the average lag is equal to 5.4 s before 03:00 on 13 May, reaching an average value of 4.7 s a few hours before the beginning of the eruption.

5. NEC conduit model

NEC is the most active crater of Mt. Etna from the acoustic point of view, whereas it has exhibited almost no eruptive activity in the last decade. Infrasound activity has been continuously recorded since the installation of the permanent network in 2006, even during non-eruptive periods. There is no visible eruptive activity at NEC during the occurrence of infrasonic events. Since NEC infrasonic events show coda composed of regularly decaying sinusoidal waveforms and sometimes harmonics (Cannata et al., 2009a; Spina et al., 2011), resonance mechanisms are considered more appropriate than other models such as a Strombolian bubble vibration model. On the other hand, no unambiguously detectable infrasound associated to explosive sources, was recognized (**Fig. 3**). Indeed, following the Strombolian bubble vibration model (e.g., Vergniolle and Brandeis, 1996) the infrasonic signal should consist of a first energetic part roughly composed of one cycle–one cycle and a half (corresponding to the bubble vibration), followed by a second part with various weaker

oscillations sometimes with higher frequency. After one single cycle of vibration (i.e. the strong impulse event in acoustic pressure) the bubble bursts emitting rather quiet higher frequencies (Vergniolle and Brandeis, 1996).

Sources related to degassing processes close to the free magma surface are likely to excite the resonance phenomena, as already hypothesised by other authors to explain resonance triggering processes (e.g. Garces and McNutt, 1997; Fee et al., 2010b).Resonance is a propagation path effect inside the conduit and is generated by multiple reflections of pressure disturbances in the fluid against boundaries (Garces and McNutt, 1997; De Angelis and McNutt, 2007). Thus, information on conduit geometry and physical properties of the fluid filling the conduit can be inferred. We hypothesized a portion of the NEC conduit behaving as a pipe resonator. Similarly to other authors (e.g. Petersen and McNutt, 2007; Fee et al., 2010b), we considered as the resonating portion of the conduit the one above the free magma surface, filled with a gas-mixture. The interface between the gas-mixture and the magma column acts as a closed termination due to the impedance contrast between the two phases. Regarding the upper end of the pipe resonator, NEC morphology should be taken into consideration. NEC shows a funnel-shaped crater at the bottom of which the upper part of the conduit is open and clearly visible (**Fig. 10a**). Nevertheless, the lack of an obstruction does not imply that it is an acoustically opened termination, as observed by several authors (e.g. Garces and McNutt, 1997; De Angelis and McNutt, 2007). Analyses of NEC infrasonic events (Spina et al., 2011), recorded during the entire 2007-2009 period, highlighted the presence of integer harmonics of the fundamental mode. Spectra with integer harmonics can be modeled by a closed-closed (or open-open) pipe resonator. For this reason, assuming that the bottom end is a closed termination, the upper end of the resonating conduit should be a closed termination, too. The parameter, on which the behavior of the termination depends (closed or open), is the impedance contrast, that is function of cross-sectional area variations (if any) of the termination and changes in fluid properties (Garces and McNutt, 1997). Therefore, if the impedance contrast in the upper end of the conduit is high, for instance due to a narrowing, this could make the termination closed. Consequently, the

small hole (with respect to the crater dimension) at the bottom of the crater could be the opening of the narrowing (**Fig. 10b**). Because of the small dimension of the conduit radius with respect to the observed infrasound wavelengths, only longitudinal modes were taken into account (Garces and McNutt, 1997). The fundamental frequency (f_0) for a closed-closed pipe resonator is equal to:

$$f_0 = \frac{c_c}{2L} \tag{1}$$

where c_c is the acoustic speed of fluid into the conduit and L is the resonating conduit portion length. By means of the **equation (1)** and taking into account a wide range of values for both c_c and L, we calculated the theoretical frequencies. As aforementioned, the higher frequency peak of infrasonic events ranges in the frequency band 1.5-2.0 Hz. **Figure 11** shows the range of variation of c_c and L for the frequency values observed. The acoustic speed in the conduit is a difficult parameter to estimate and is given by:

$$c_c = \sqrt{\gamma R_g T} \tag{2}$$

where γ is the heat capacity ratio, R_g the gas constant and T the temperature for the mixture. For instance, Sahetapy-Engel et al. (2008) and Weill et al. (1992) considered a fluid temperature in the conduit of 1173° K for both Stromboli and Santiaguito. Fee et al. (2010b) by means of FLIR imagery estimated an average temperature inside the cavity of Halema'uma'u of about 470° K. Other authors also performed some measurements of lava temperature by FLIR, obtaining for instance ~1100-1200° K at Stromboli (Harris et al., 2005) and ~1000-1300° K at Etna (Bailey et al., 2006).

With the aim of constraining the acoustic speed, we used chemical compositions of gas emitted by NEC during 2008 and 2009 (La Spina et al., 2010), and applied the ideal mixing theory, as reported in Morrissey and Chouet (2001). The acoustic speeds were calculated by considering temperatures equal to 300°, 800° and 1200° K and the associated R_g and γ values. In particular, for each gas species, the R_g and γ values at 300° K were found in Serway and Jewett (2006) and at 800° and 1200° K in Morrissey and Chouet (2001). Therefore, applying **equation (2)**, we obtained an acoustic speed ranging between 400 and 750 m/s.

We took into consideration the time interval in which infrasonic events were characterized by both the higher and lower frequency components (16:00-24:00 of 12 May; **Fig. 4a**). Therefore, taking into account the above calculated range of acoustic speed and the observed higher frequency peak in this time interval (2 Hz), the length of the resonating conduit portion ranges roughly between 100 and 200 m (**Fig. 11**).

Segments of pipes, all of whose dimensions are sufficiently small compared to the wavelengths, can be considered as lumped acoustic elements. A simple example of a lumped acoustic system is the Helmholtz resonator. It consists of a cavity connected with the outside space through a narrow neck or through an opening (Alster, 1972). As aforementioned, infrasonic events recorded on 13 May also contain a lower frequency band at 0.4-0.7 Hz. In this case, since the wavelength (~820-1430 m, with an acoustic speed of 575 m/s, the mean value of the aforementioned c_c range) is much longer than the dimension of the conduit, we modeled this lower frequency band as due to a Helmholtz resonance. We consider the conduit as the rigid walled cavity and the narrowing in its upper part acting as a neck (**Fig. 10b**). Such a cavity geometry generates a resonance frequency equal to (Kinsler et al., 1982):

$$f = \frac{c_c}{2\pi}\sqrt{\frac{S}{Vk'}} \qquad (3)$$

where S is the area of the neck (narrowing), V is the cavity volume (conduit) and k' is the neck effective length ($k' = a + 1.45 * l$, where a is the neck length and l is the neck radius). Most of the parameters, which the Helmholtz resonator frequency depends on, are unknown. We only have a measure of the neck radius, estimated at 15 m. First, we calculated the Helmholtz resonator theoretical frequencies fixing the acoustic speed in the conduit and the conduit length (575 m/s and 150 m, respectively), but systematically changing both neck length and conduit radius. Results are shown in **Figure 12**, which demonstrate that the frequency variation is more influenced by the conduit radius with respect to the neck length. Hence, the next step was an attempt to estimate the conduit radius. As aforementioned, the higher spectral peak observed on 12 May between 16:00 and 24:00, modeled as a pipe resonator frequency, led us to obtain a range of probable conduit length of 100-200 m. On the basis of this observation, we applied the Helmholtz resonator model to the lower frequency peak (0.4 Hz), observed during the same interval (16:00-24:00 on 12 May). Therefore, we solved the **equation (3)** for the conduit radius and, fixing S and l at ~700 m^2 and 15 m, respectively, obtained a range of values (25-75 m) in relation to the inferred conduit length and acoustic speed. Successively, we performed the calculation for the following period (00:00-08:00 on 13 May), where the frequency peak reached 0.7 Hz, obtaining a radius ranging from 15 to 45 m. The overlap between these value intervals (25-75 m and 15-45 m) is 25-45 m and should represent a reasonable range for the conduit radius. Bonaccorso and Davis (1999; and references therein) assumed a radius of 25 m to model the ground deformation for an explosive eruption occurring in December 1995 at NEC.

Therefore, on the basis of our interpretation of the NEC events, both the spectral components of which they are made are due to propagation effects (the lower and the higher ones to Helmholtz and pipe resonances, respectively). The source likely triggering the resonance (releases of gas at the free magma surface) does not generate clear infrasound signals. In the proposed model the upper end of the pipe resonator is considered closed because of the conduit narrowing. Such a narrowing, equal

to ~10-35% of the conduit section (considering conduit radius of 45-25 m, respectively), allows the atmosphere coupling and the infrasonic radiation. The portion of acoustic energy transmitted and reflected through the narrowing can be quantified by estimating the power transmission (*Tp*) and reflection (*Rp*) coefficients (Raichel, 2006):

$$Tp = \frac{4}{4\cos^2 ka + \left(\frac{S}{A} + \frac{A}{S}\right)^2 \sin^2 ka} \tag{4}$$

$$Rp = 1 - Tp \tag{5}$$

where k is the wave number which equals to $2\pi/\lambda$ (λ is the wavelength), A is the cross-sectional area of the conduit. Such coefficients range from 0 to 1 and depend on the neck length, the ratio between the cross-sectional areas of the conduit and the narrowing, as well as on the acoustic frequency. In **Figure 13** the variation of *Tp* and *Rp* with frequency, assuming c_c equal to 575 m/s and conduit radius of 25 and 45 m (**Fig. 13 a** and **b**, respectively), is plotted. It can be noted how, at the NEC event frequencies, a good amount of acoustic energy is transmitted through the narrowing. Further, since the transmission coefficient decreases with increasing frequency, such a structure behaves as a low-pass filter.

The **Figure 14** shows the relationship between Helmholtz / pipe resonance frequency peaks and the conduit length assuming a fixed c_c value of 575 m/s. As above described, in the proposed model a conduit portion works contemporaneously as a Helmholtz cavity and a closed-closed pipe, to explain the coexistence of two spectral components. A well-known natural system can behave in a similar way: the vocal tract. Indeed, in the case of the vowel “i” the jaw and the tongue body are raised, creating a narrow front cavity, and the tongue body is moved forward, enlarging the back cavity (e.g. Diehl, 2008). Therefore, this configuration, with a constriction in the middle, gives rise

to two cavities: the front cavity behaving as an open-closed pipe, and the back cavity as both closed-closed pipe and Helmholtz resonator (e.g. Johnson, 1997; Diehl, 2008). The coexistence of the three resonance peaks creates the vowel "i" spectrum.

Successively, we analyzed temporal variations of seismo-infrasonic event features, taking place during the 12 hours before the eruption onset. During this time interval the higher frequency component of infrasonic events disappeared; hence we focused on the frequency increase of the lower peak (**Fig. 4a, c**) and on the decrease of the time lag between seismic and infrasonic events (**Fig. 9**). We applied the Helmholtz resonator model, using for the conduit radius the mean value of the aforementioned range (25-45 m), and calculated the theoretical frequencies in function of L and c_c. **Figure 15** shows that both decrease of L and/or increase of c_c can be responsible for the observed frequency increase (from 0.4 to 0.7 Hz). We tend to discard the lower values of the range of c_c shown in **Figure 15** because they imply such low conduit length values (down to 30 m) that, assuming the conduit radius comprised between 25 and 45 m, pipe resonance is not plausible.

The lag between seismic and infrasonic events and its temporal variation have been used in literature to determine the depth of the source triggering the resonance (e.g. Ripepe and Braun, 1994; Ripepe et al., 2001a; Gresta et al., 2004; Petersen and McNutt, 2007). To do so, seismic and infrasonic sources can be considered either co-located, generally coinciding with the free magma surface inside the conduit, or not. If the latter, the delay between seismic and infrasonic onsets is related to a seismic pressure wave ascending through the conduit (Ishihara, 1985) or to a rising gas slug (Ripepe et al., 2001a). In this work, the similarity between the waveform and spectral contents of seismic and infrasonic signals, suggesting a common source (e.g. Ripepe et al., 1996; Matoza et al., 2010), makes the model with co-located seismic-infrasonic sources more reasonable. In order to investigate the time lag decrease from 5.4 to 4.7 s, occurring between 00:00 and 08:00 on 13 May, we used the approach of Petersen and McNutt (2007). Infrasound waves cover the distance between the source and the crater rim with speed c_c, depending on the property of the fluid filling the

conduit, then they propagate in the atmosphere as far as the infrasonic station with acoustic speed equal to 340 m/s (c). On the other hand, seismic waves travel in the rocks in between the source and the seismic station with (P-wave) velocity v. Therefore, the lag is given by:

$$time\ lag = \frac{x}{c} + \frac{z}{c_c} - \frac{d}{v} \quad (6)$$

where x is the distance between the crater rim and the microphone, z is the depth of the magma free surface (source) with respect to the crater rim, and d is the distance between the source and the seismic station (see **Figure 10b**). Considering the seismo-infrasonic events recorded at station EBEL, located ~2000 m away from NEC, we calculated the theoretical time lags by systematically changing source altitude (z), c_c values and v (**Fig. 16**). First of all, it was noted how the maximum seismic velocity, on the basis of which a seismic-infrasonic time lag of 4.7 s can be obtained, is ~1500 m/s. Indeed, the contour line representing 4.7 s disappeared in **Figure 16f**. Because of the expected shallowness of the seismic-infrasonic sources in this study, we cannot use results from tomographic studies at Mt. Etna to constrain the seismic velocity. In any case, the obtained seismic velocity upper limit (~1500 m/s) concurs with the evidences of near-surface (a few hundred meters) low seismic velocities, which are common in volcanic environments and have been reported in many papers (e.g. Saccorotti et al., 2004; Bean et al., 2008). In all the considered cases in **Figure 16**, it is evident that a time lag decrease from 5.4 to 4.7 s cannot be due only to an increase of c_c alone, but necessarily implies a shallowing of the source. For instance, if we consider the mean value of the range of c_c above mentioned (575 m/s) and a seismic velocity of 1300 m/s, and take into account the time lag value shortly before the beginning of the eruption (4.7 s), we obtain a source altitude equal to 3180 m a.s.l. (**Fig. 16c**). We also considered the hypothesis in which the sources of seismic and infrasound events are non co-located in order to validate these results. In this case the seismic source should be located at a vertical distance below the infrasonic source which is

instead located at the free magma surface. Under this hypothesis, the **equation (6)** of time lag also depends on the ratio h/U_b, where h is the vertical distance between the seismic and infrasound sources and U_b is the velocity of a gas slug ascending through the magma into the conduit. Taking into account the observed time lags and a U_b value of 50 m/s (Gresta et al., 2004 and reference therein), to obtain a vertical distance between the sources (h) of 50 m, P-wave velocity cannot be higher than 0.8 km/s. This allows definitely discarding the hypothesis of non co-located seismo-infrasound sources.

On the basis of the estimated source altitude, for the same time interval, and hence considering a peak frequency equal to 0.7 Hz, we used the same value of c_c to extract a value of conduit length by means of the Helmholtz resonator (**Fig. 15**), obtaining a 90 m long resonator. Assuming 3330 m a.s.l. as the crater rim altitude and a ~70 m deep funnel-shaped crater, a 90 m long resonator is equivalent to a source altitude of 3170 m a.s.l. It is noteworthy that the depth value of the source of the seismo-infrasonic events calculated by means of the Helmholtz resonance model is consistent with the one obtained using the time lag. Under the assumption that the lag variation observed a few hours before the eruption is largely due to a shallowing of the magma column level, and considering a constant value of sound velocity (575 m/s), the fragmentation level altitude inside the conduit should have changed from ~2800 (during 12 May) to 3180 m a.s.l. (morning of 13 May) (**Fig. 16c**). Finally, we evaluated the fragmentation level altitude during 12 May also by applying the Helmholtz resonator equation: assuming 0.4 Hz we obtained a conduit length of 260 m, which, considering a ~70 m deep crater, corresponds to ~3000 m a.s.l. Nevertheless, the mismatch between this value and the previous one computed by the lag may simply be due to inaccuracy in the peak frequency estimation. Since the duration of the infrasonic events is about 10-15 s, the window length used to estimate the peak frequency was fixed to 10 s, and consequently the spectral resolution was roughly equal to 0.1 Hz. Indeed, if 0.3 Hz, instead of 0.4 Hz, is used in the calculation of the Helmholtz resonator length, we obtain a value of 460 m (**Fig. 15**), and therefore a

fragmentation level altitude of 2800 m a.s.l., in agreement with the one evaluated by the lag approach.

Finally, it is worth noting that, although the estimated depth values of the fragmentation level depend on several assumptions (e.g. seismic velocity, acoustic speed in the conduit) and hence can be imprecise, the waveform and spectral variations of the NEC events undoubtedly suggest a shallowing of the magma level inside the NEC conduit a few hours before the beginning of the eruption.

6. Discussion

In this work, we analyzed 157 infrasound events and the corresponding seismic signals detected during 12-13 May 2008, and preceding the 2008-2009 eruption begun on the morning of 13 May.

The recharging phase preceding the 2008-2009 flank eruption started in 2007 and was evidenced by a positive areal dilatation and several lava fountain episodes (Bonaccorso et al., 2011). From January 2008 to the beginning of the eruption, the energy release related to volcano-tectonic earthquakes underwent an acceleration, initially due to deep earthquakes (focal depth of 10-20 km b.s.l.) and successively to shallower ones. In the same period, the GPS network measured inflation processes, at first at relatively low altitude before reaching the higher altitude in March (Di Grazia et al., 2009).

Changes in seismo-volcanic signals occurred during the two weeks preceding the onset of the eruption. The LP events, located from January beneath BN crater, became deeper and underwent an increase in both number and amplitude after 4 May. In the same period the volcanic tremor, located beneath the central craters, deepened as well, and changed becoming monochromatic (Patanè et al., 2011). All the LP and volcanic tremor variations preceded and heralded the lava fountain taking place on 10 May at SEC (Patanè et al., 2011). Such seismo-volcanic changes were interpreted as the arrival of gas-rich magma up to the shallower portion of plumbing system (Patanè et al., 2011).

Focusing on the time period after the lava fountain and before the beginning of the eruption, further changes in the seismo-volcanic signals were observed. From the early afternoon on 12 May, a gradual migration of the volcanic tremor epicentres from BN toward NEC and the NE Rift took place (Patanè et al., 2011). In particular, the source of the volcanic tremor was located under the NEC at about 1.5 km below the crater (Patanè et al., 2011).

The infrasonic and seismic signals, making up our data-set, are likely to be generated by the same source as suggested by the similar frequency content, waveforms and epicentral location (**Figs. 5, 6** and **7**). The importance of these events is related to both the peculiar infrasonic low frequency component (<0.7 Hz), rarely recorded at Etna before, and the significant changes (mainly affecting infrasonic spectral content and time lag between seismic and infrasonic signals) taking place a few hours before the eruption onset (**Figs. 4** and **9**).

Low frequency components were already observed at Mt. Etna during 2001 eruptive activity by Vergniolle and Ripepe (2008). They described an equivalent frequency of ~0.5 Hz in infrasonic signals related to three wavelet-like peaks in acoustic pressure separated by 2 s with a period of 0.76 s (1.3 Hz), which were attributed to sloshing waves induced at the top of the magma column by a large bubble approaching the surface. In confirmation of this, such a sloshing wave signal was followed by a strong explosion at SEC caused by the bubble bursting at the free magma surface. The marked spectral and waveform differences between these 2001 signals and our data make this interpretation unsuitable for NEC events. In addition, taking into account a conduit with radius of 25 m (see **section 5**) and using the equations reported in Vergniolle et al. (1996), the first radial and angular modes related to sloshing waves have frequencies of 0.19 and 0.13 Hz, respectively, while we observed 0.4-0.7 Hz for NEC events. Moreover, since the sloshing waves in a conduit are likely related to uprising large bubbles, as hypothesized by Vergniolle and Ripepe (2008), the lack of clear strong explosion signals right after the observed low frequency NEC events further supports the unsuitability of sloshing wave model to our data.

Volcanoes around the world have demonstrated that many different phenomena are able to produce infrasound, whose sources have been modelled. The interplay between the parameters at the basis of each model (e.g. geometrical features, chemical-physical properties of magma and surrounding rocks) may explain the observation of the same frequency content for different kinds of activity. We believe that this is the explanation for the similar frequencies observed by Vergniolle and Ripepe (2008) with respect to those reported in this work.

It is noteworthy that volcanic tremor source migration took place at the same time as the occurrence rate of seismo-infrasonic events reached the maximum value (22:00 on 12 May, **Fig. 2c**). All these features suggest that the seismo-infrasonic events are closely linked to the impending eruption, even if they are located at NEC and the eruptive activity occurred at a fissure opened up on the upper eastern flank of the volcano.

The infrasonic component of these seismo-infrasonic events is characterized by two frequency bands, 0.4-0.7 and 1.5-2.0 Hz, whose sources were attributed to resonance phenomena inside the conduit. The conduit portion, responsible for such signals, is likely bounded by the magma fragmentation level, at the bottom, and a narrowing, at the top, and is filled with a gas-mixture. Sources, close to the free magma surface, related to degassing processes, trigger propagation effects (such as resonance phenomena) because of the interaction with the conduit. In particular, on the basis of the waveform and spectral features of the two aforementioned frequency bands, we inferred the superposition of two resonance phenomena: a closed-closed pipe resonance, producing the higher frequency peak (1.5-2.0 Hz), and a Helmholtz resonance, generating the lower frequency peak (0.4-0.7 Hz) (**Fig. 10b**). On the basis of both spectral features and time lag between seismic and infrasound components, inferences on the geometrical features of NEC conduit were made. In particular, ranges for the conduit radius values and for the depth of the magma free surface, where the source triggering the resonance is supposed to be sited, were inferred. Variations in such seismo-infrasonic events can provide information on the magma column dynamics inside the shallow part of NEC conduit. The aforesaid spectral variations, together with the decreasing

seismic-infrasonic time lag, occurring during 12-13 May, are clearly included in the framework of the seismo-volcanic signal changes sometimes observed before and during volcanic eruptions, at Etna and other volcanoes as well (e.g. Kobayashi et al., 2005; Sciotto et al., 2011). The decreasing pattern of the time lag measured a few hours before the eruption is to be ascribed to the magma free surface shallowing, even if we cannot exclude that c_c changes could contribute to the variation. Similarly, also the increase of the infrasound dominant frequencies was interpreted as resulting from the shortening of both pipe and Helmholtz resonators.

According to Aloisi et al. (2009) and Bonaccorso et al. (2011), the 2008-2009 eruption was fed by an intrusion following the path of the central conduit in the first part of the intrusion up to a shallow storage zone (below 1.5-2.0 km a.s.l.) and then breaking off toward the east in the shallow part. As aforementioned, given that both the occurrence and variations of the analyzed seismo-infrasonic events are closely time-related to the eruption onset, we can infer that the NEC conduit is directly linked to some portions of such plumbing system (for instance to the shallow storage zone at 1.5-2.0 km a.s.l.) feeding the 2008-2009 eruption (**Fig. 10c**). Proof of a branched shallow plumbing system has already been found at Etna by Marchetti et al. (2009), La Spina et al. (2010) and Sciotto et al. (2011). In particular, La Spina et al. (2010) modelled a shallow plumbing system in which NEC conduit is a branch of the central feeding conduit.

However, it is worth noting that the shallow interconnections among the summit craters should be considered time-dependent. Indeed, previous studies, based on volcanological, petrological and volcanic tremor data acquired before 1990, suggested the relative independence of the NEC conduit with respect to the central feeding system (Schick et al., 1982; Gresta et al., 1991). The temporal variability of the conduit connection does not only involve NEC but also other summit craters. For instance, Corsaro and Pompilio (2004), making an integrated study of compositional, volcanological and geophysical data, found that during 1995-1999 SEC products were more highly differentiated than those of the other craters, while, from the beginning of 1999, the SEC volcanics progressively changed in composition, becoming similar to those of the other craters. These authors

ascribed this variation to severe modifications of the shallow plumbing system. Also our model is time–dependent and is only valid for NEC in this peculiar period characterized by degassing without visible activity. It is highly possible that future volcanic eruptions at this crater will modify the main characteristics of conduit geometry, which are the fundamental boundary conditions of our model.

In light of the observed NEC connection, the change in the magma level inside the NEC conduit, inferred on the basis of spectral and time lag variations, can be linked to the pressure increase inside this plumbing system. Indeed, if we consider a simple plumbing system made up of a magma chamber connected to a vertical open-conduit, in equilibrium conditions the pressure inside the chamber must be balanced by the magmastatic pressure of the conduit (e.g. Witham and Llewellin, 2006). Therefore, a pressure increase inside the shallow storage zone at 1.5–2.0 km a.s.l. can cause the magma to flow from the chamber into NEC conduit, with a consequent magma level increase inside it. Taking into account the fragmentation level increase, estimated at equal to ~ 200-400 m (see **section 5**), and considering a constant value of magma density inside the conduit in the range 700-2700 kg/m^3 (gas-magma foam and bubble-free magma, respectively; e.g. Pinkerton et al., 2002), we obtain a pressure increase inside the plumbing system of ~1.5-11 MPa, preceding the onset of the eruption by a few hours. Although there are major uncertainties in this evaluation, mainly related to the above assumptions, the magnitude order of such a pressure increase value may be considered reliable. Such a pressure increase is able to fracture rocks (e.g. Tait et al., 1989) and is also roughly consistent with the driving pressure value of 13 MPa, considered responsible for the intrusive process preceding the 2008-2009 eruption by Currenti et al. (2011).

A pressure increase inside the plumbing system can be caused by different mechanisms, such as magma input from a deeper source, gas exsolution and dynamical stress transfer (e.g. McLeod and Tait, 1999; Cannata et al., 2010). These processes may be related to each other, too. For instance, the heating of the original magma by new hot input lowers the volatile solubility, hence promoting gas exsolution (McLeod and Tait, 1999). Similarly, small pressure changes, associated with

dynamic stresses in a crystallizing magma that is close to critical supersaturation, should be able to trigger a significant increase in bubble nucleation, leading to a marked pressure increase (Cannata et al., 2010). On the basis of the data shown in this work, we cannot pinpoint the exact phenomenon leading to the plumbing system pressure increase. However, since such a variation took place in a relatively short interval (a few hours), slow processes, such as crystallization increasing the concentration of volatile in the melt, can be excluded.

Finally, it is noteworthy that the above analyzed variations of seismo-infrasonic events, occurring during the night between 12 and 13 May, preceded the VT seismic swarm, located NE of the summit craters, and the accelerating ground deformation starting from 08:39 on 13 May. Such phenomena, that similarly to the seismo-infrasonic event variations were caused by a pressure increase inside the plumbing system, were followed at ~9:30 by the opening of an eruptive fissure and then by the beginning of the 2008-2009 eruption.

7. Concluding remarks

The seismo-volcanic events, occurring a few hours before the beginning of the May 2008 eruption, have been analyzed in this study. The following points summarize the main findings:

- The shallower portion of the plumbing system feeding NEC was modelled by seismic and infrasound data. Pipe and Helmholtz resonances were supposed contemporaneously active at NEC, giving rise to a higher and a lower frequency component in the infrasound signal, respectively.
- The occurrence of seismo-infrasonic events located at NEC during the hours preceding the eruption, together with the variation of their features, led us to infer a link between NEC conduit and the plumbing system feeding the activity at the eruptive fissure on 13 May 2008.
- On the basis of variations over time of both spectral features and seismic-infrasonic time lag, shallowing phenomena of the free magma surface inside NEC conduit were inferred.

- The ascent of magma column is likely due to pressure increase in the plumbing system that preceded/accompanied the VT seismic swarm and the acceleration of ground deformation in the summit area.

In conclusion, analyses of seismo-infrasonic events, preceding the 13 May 2008 eruption, have proved to be a useful tool in detecting instability in the shallow plumbing system in advance with respect to other geophysical parameters. Such multi-parametric approaches may be valuable techniques to be integrated in the monitoring of open conduit volcanoes throughout the world.

Acknowledgements

We are indebted to Luciano Scuderi for the technical management of the Mt. Etna Infrasonic Network and for performing laboratory tests. We are grateful to the Editor Jurgen Neuberg, Maurizio Ripepe and an anonymous reviewer for their useful suggestions that greatly improved the paper. We thank S. Conway for revising the English language of this manuscript.

References

Aiuppa, A., Cannata, A., Cannavò, F., Di Grazia, G., Ferrari, F., Giudice, G., Gurrieri, S., Liuzzo, M., Mattia, M., Montalto, P., Patanè, D., Puglisi, G., 2010. Patterns in the recent 2007–2008 activity of Mount Etna volcano investigated by integrated geophysical and geochemical observations. Geochem. Geophys. Geosyst. 11, Q09008, doi:10.1029/2010GC003168.

Aloisi, M., Bonaccorso, A., Cannavò, F., Gambino, S., Mattia, M., Puglisi, G., Boschi, E., 2009. A new dike intrusion style for the Mount Etna May 2008 eruption modelled through continuous tilt and GPS data. Terra Nova 21, 316–321, doi:10.1111/j.1365-3121.2009.00889.x.

Alster, M., 1972. Improved calculation of resonant frequencies of Helmholtz resonators. J. Sound Vib. 24, 63–85.

Arrowsmith, S., Johnson, J., Drob, D., Hedlin, M., 2010. The Seismo-Acoustic Wavefield: A new paradigm in studying geophysical phenomena. Review of Geophysics, doi:10.1029/2010RG000335.

Bailey, J., Harris, A., Dehn, J., Calvari, S., Rowland, S., 2006. The changing morphology of an open lava channel on Mt. Etna. Bull. Volcanol. 68, 497–515.

Bean, C., Lokmer, I., O'Brien, G., 2008, Influence of near-surface volcanic structure on long-period seismic signals and on moment tensor inversions: Simulated examples from Mount Etna. J. Geophys. Res. 113, B08308, doi:10.1029/2007JB005468.

Behncke, B., Branca, S., De Beni, E., Proietti, C., 2009. Eruzione 2008–09 dell'Etna: Mappatura del campo lavico (in Italian). Internal Rep. WKRVG20090526, Ist. Naz. Di Geofis. e Vulcanol., Rome. (Available at http://www.earth-prints.org/handle/2122/5551)

Bonaccorso, A., Davis, P. M., 1999. Models of ground deformation from vertical volcanic conduits with application to eruptions of Mount St. Helens and Mount Etna. J. Geophys. Res. 104, 10531–10542.

Bonaccorso, A., Bonforte, A., Calvari, S., Del Negro, C., Di Grazia, G., Ganci, G., Neri, M., Vicari, A., Boschi, E., 2011. The initial phases of the 2008–2009 Mount Etna eruption: A multidisciplinary approach for hazard assessment. J. Geophys. Res. 116, doi:10.1029/2010JB007906.

Cannata, A., Montalto, P., Privitera, E., Russo, G., Gresta, S., 2009a. Tracking eruptive phenomena by infrasound: May 13, 2008 eruption at Mt.Etna. Geophys. Res. Lett. 36, L05304, doi:10.1029/2008GL036738.

Cannata, A., Montalto, P., Privitera, E., Russo, G., 2009b. Characterization and location of infrasonic sources in active volcanoes: Mt. Etna, September-November 2007. J. Geophys. Res. 114, B08308, doi:10.1029/2008JB006007.

Cannata, A., Di Grazia, G., Montalto, P., Aliotta, M., Patanè, D., Boschi, E., 2010. Response of Mount Etna to dynamic stresses from distant earthquakes. J. Geophys. Res. 115, B12304, doi:10.1029/2010JB007487.

Cannata, A., Sciotto, M., Spina, L., Spampinato, L., 2011. Insights into explosive activity at eruptive fissure closely-spaced vents by infrasound signals: example of Mt. Etna 2008 eruption. J. Volcanol. Geotherm. Res. 208, 1–11.

Caplan-Auerbach, J., Bellesiles, A., Fernandes, J. K., 2009. Estimates of eruption velocity and plume height from infrasonic recordings of the 2006 eruption of Augustine Volcano, Alaska. J. Volcanol. Geotherm. Res. 189, 12-18, doi:10.1016/j.jvolgeores.2009.10.002.

Currenti, G., Napoli, R., Di Stefano, A., Greco, F., Del Negro, C., 2011. 3D integrated geophysical modeling for the 2008 magma intrusion at Etna: Constraints on rheology and dike overpressure Physics of the Earth and Planetary Interiors 185, 44-52.

De Angelis, S., McNutt, S. R., 2007. Observations of volcanic tremor during the January-February 2005 eruption of Mt. Veniaminof, Alaska. Bull. Volcanol. 69, 927–940.

Di Grazia, G., Cannata, A., Montalto, P., Patanè, D., Privitera, E., Zuccarello, L., Boschi, E., 2009. A multiparameter approach to volcano monitoring based on 4D analyses of seismo-volcanic and acoustic signals: the 2008 Mt.Etna eruption. Geophys. Res. Lett. 36, L18307, doi:10.1029/2009GL039567.

Diehl, R. L., 2008. Acoustic and auditory phonetics: the adaptive design of speech sound systems. Phil. Trans. R. Soc. B 363, 965–978.

Fee, D., Steffke, A., Garces, M., 2010a. Characterization of the 2008 Kasatochi and Okmok eruptions using remote infrasound arrays. J. Geophys. Res. 115, D00L10, doi:10.1029/2009JD013621.

Fee, D., Garcés, M., Patrick, M., Chouet, B., Dawson, P., Swanson, D., 2010b. Infrasonic harmonic tremor and degassing bursts from Halema'uma'u Crater, Kilauea Volcano, Hawaii. J. Geophys. Res. 115, B11316, doi:10.1029/2010JB007642.

Garces, M. A., McNutt, S. R., 1997. Theory of the airborne sound field generated in a resonant magma conduit. J. Volcanol. Geotherm. Res. 78, 155–178.

Goto, A., Johnson, J. B., 2011. Monotonic infrasound and Helmholtz resonance at Volcan Villarrica (Chile). Geophys. Res. Lett. 38, L06301, doi:10.1029/2011GL046858.

Gresta, S., Montalto, A., Patanè, G., 1991. Volcanic tremor at Mount Etna (January 1984-March 1985): its relationship to the eruptive activity and modelling of the summit feeding system. Bull. Volcanol., 53, 309-320.

Gresta, S., Ripepe, M., Marchetti, E., D'Amico, S., Coltelli, M., Harris, A. J. L., Privitera, E., 2004. Seismoacoustic measurements during the July – August 2001 eruption at Mt. Etna volcano, Italy. J. Volcanol. Geotherm. Res. 137, 219 – 230.

Hagerty, M. T., Schwartz, S. Y., Garcés, M. A., Protti, M., 2000. Analysis of seismic and acoustic observations at Arenal volcano, Costa Rica, 1995–1997. J. Volcanol. Geotherm. Res. 101, 27–65, doi:10.1016/S0377-0273(00)00162-1.

Harris, A., Dehn, J., Patrick , M., Calvari, S., Ripepe, M., Lodato, L., 2005. Lava effusion rates from hand-held thermal infrared imagery: an example from the June 2003 effusive activity at Stromboli. Bull. Volcanol. 68, 107–117.

Ishihara, K., 1985. Dynamical analysis of volcanic explosion. J. Geodyn. 3, 327–349.

Johnson, K., 1997. Acoustic and Auditory Phonetics. Malden, MA, Blackwell Publishers.

Johnson, J. B., 2005. Source location variability and volcanic vent mapping with a small-aperture infrasound array at Stromboli Volcano, Italy. Bull. Volcan. 67, 1–14.

Johnson, J. B., Aster, R. C., 2005. Relative partitioning of acoustic and seismic energy during Strombolian eruptions. J. Volcanol. Geotherm. Res. 148, 334–354, doi:10.1016/j.jvolgeores.2005.05.002.

Kinsler, L. E., Frey, A. R., Coppens, A. B., Sanders, J. V., 1982. Fundamentals of Acoustics. Third Edition ed., John Wiley and Sons, 480 pp.

Kobayashi, T., Ida, Y., Ohminato, T., 2005. Small inflation sources producing seismic and infrasonic pulses during the 2000 eruptions of Miyake-jima, Japan. Earth Planet. Sci. Lett. 240, 291–301.

Langer, H., Falsaperla, S., Messina, A., Spampinato, S., Behncke, B., 2011. Detecting imminent eruptive activity at Mt Etna, Italy, in 2007-2008 through pattern classification of volcanic tremor data. J. Volcanol. Geotherm. Res. 200, 1–17, doi: 10.1016/j.jvolgeores.2010.11.019.

La Spina, A., Burton, M., Salerno, G. G., 2010. Unravelling the processes controlling gas emissions from the Central and Northeast craters of Mt. Etna. J. Volcanol. Geotherm. Res. 198, 368-376, doi:10.1016/j.jvolgeores.2010.09.018.

Marchetti, E., Ripepe, M., Ulivieri, G., Caffo, S., Privitera, E., 2009. Infrasonic evidences for branched conduit dynamics at Mt. Etna volcano, Italy. Geophys. Res. Lett. 36, L19308, doi:10.1029/2009GL040070.

Matoza, R. S., Garces, M. A., Chouet, B., D'Auria, L., Hedlin, H., De Grooth-Hedlin, C., Waite, G. P., 2009. The source of infrasound associated with long-period events at Mount St. Helens. J. Geophys. Res. 114, doi:10.1029/2008JB006128.

Matoza, R. S., Fee, D., Garcés, M. A., 2010. Infrasonic tremor wavefield of the Pu'u'Ō'ō crater complex and lava tube system, Hawaii, in April 2007. J. Geophys. Res. 115, B12312, doi:10.1029/2009JB007192.

McLeod, P., Tait, S., 1999. The growth of dykes from magma chambers. J. Volcanol. Geotherm. Res. 92, 231–246.

Morrissey, M. M., Chouet, B. A., 2001. Trends in long-period seismicity related to magmatic fluid compositions. J. Volcanol. Geotherm. Res. 108, 265–281.

Napoli, R., Currenti, G., Del Negro, C., Greco, F., Scandura, D., 2008. Volcanomagnetic evidence of the magmatic intrusion on 13th May 2008 Etna eruption. Geophys. Res. Lett. 35, L22301, doi:10.1029/2008GL035350.

Patanè, D., Aliotta, M., Cannata, A., Cassisi, C., Coltelli, M., Di Grazia, G., Montalto, P., Zuccarello, L., 2011. Interplay between Tectonics and Mount Etna's Volcanism: Insights into the Geometry of the Plumbing System. In: Schattner, U. (Ed.), New Frontiers in Tectonic Research - At the Midst of Plate Convergence. Intech open access publisher.

Petersen, T., McNutt, S. R., 2007. Seismo-acoustic signals associated with degassing explosions recorded at Shishaldin Volcano, Alaska, 2003–2004. Bull. Volcanol. 69, 527–536, doi:10.1007/s00445-006-0088-z.

Pinkerton, H., Wilson, L., Macdonald, R., 2002. The transport and eruption of magma from volcanoes: a review. Contemp. Phys. 43, 197–210.

Pistolesi, M., Delle Donne, D., Pioli, L., Rosi, M., Ripepe, M., 2011. The 15 March 2007 explosive crisis at Stromboli volcano, Italy: Assessing physical parameters through a multidisciplinary approach. J. Geophys. Res. 116, B12206, doi:10.1029/2011JB008527.

Raichel, D.R., 2006. The science and applications of acoustics. New York, Springer.

Ripepe, M., Braun, T., 1994. Air-wave phases in strombolian explosion quake seismograms: a possible indicator for the magma level? Acta Vulcanologica 5, 201-206.

Ripepe, M., Poggi, P., Braun, T., Gordeev, E., 1996. Infrasonic waves and volcanic tremor at Stromboli. Geophys. Res. Lett. 23, 181–184, doi:10.1029/95GL03662.

Ripepe, M., Ciliberto, S., Schiava, M. D., 2001a. Time constraints for modeling source dynamics of volcanic explosions at Stromboli. J. Geophys. Res. 106, 8713–8727, doi:10.1029/2000JB900374.

Ripepe, M., Coltelli, M., Privitera, E., Gresta, S., Moretti, M., Piccinini, D., 2001b. Seismic and infrasonic evidences for an impulsive source of the shallow volcanic tremor at Mt. Etna, Italy. Geophys. Res. Lett. 28(6), 1071–1074, doi:10.1029/2000GL011391.

Saccorotti, G., Zuccarello, L., Del Pezzo, E., Ibanez, J., Gresta, S., 2004. Quantitative analysis of the tremor wavefield at Etna Volcano. J. Volcanol. Geotherm. Res. 136, 223–245, doi:10.1016/j.jvolgeores.2004.04.003.

Sahetapy-Engel, S. T., Harris, A. J. L., Marchetti, E., 2008. Thermal, seismic and infrasound observations of persistent explosive activity and conduit dynamics at Santiaguito lava dome, Guatemala. J. Volcanol. Geotherm. Res. 173, 1–14.

Schick, R., Cosentino, M., Lombardo, G., Patanè, G., 1982. Volcanic tremor at Mt. Etna. A brief description. Mem. Soc. Geol. Ital. 23, 191-196.

Sciotto, M., Cannata, A., Di Grazia, G., Gresta, S., Privitera, E., Spina, L., 2011. Seismoacoustic investigations of paroxysmal activity at Mt. Etna volcano: New insights into the 16 November 2006 eruption. J. Geophys. Res. 116, B09301, doi:10.1029/2010JB008138.

Serway, R. A., Jewett, J. W., 2006. Principles of physics: a calculus-based text. Brooks/Cole, Belmont, CA, USA.

Spina, L., Cannata, A., Privitera, E., Vergniolle, S., Ferlito, C., Gresta, S., Montalto, P., Sciotto, M., 2011. Inside the shallow Mt. Etna plumbing system from analysis of infrasonic signals (August 2007-December 2009). Geophysical Research Abstracts, vol. 13, EGU2011-8476.

Tait, S., Jaupart, C., Vergniolle, S., 1989. Pressure, gas content and eruption periodicity of a shallow, crystallising magma chamber. Earth Planet. Sci. Lett. 92, 107-123.

Vergniolle, S., Brandeis, G., 1996. Strombolian explosions: 1. A large bubble breaking at the surface of a lava column as a source of sound. J. Geophys. Res. 101, 20433–20448

Vergniolle, S., Brandeis, G., Mareschal, J. C., 1996. Strombolian explosions: 2. Eruption dynamics determined from acoustic measurements. J. Geophys. Res. 101, 20449–20465.

Vergniolle, S., Ripepe, M., 2008. From Strombolian explosions to fire fountains at Etna Volcano (Italy): what do we learn from acoustic measurements? Geol. Soc. London, Special Publications 307, 103–124.

Weill, A., Brandeis, G., Vergniolle, S., Baudin, F., Bilbille, J., Fevre, J., Piron, B., Hill, X., 1992. Acoustic sounder measurements of the vertical velocity of volcanic jets at Stromboli volcano. Geophys. Res. Lett. 19, 2357–2360.

Witham, F., Llewellin, E.W., 2006. Stability of lava lakes. J. Volc. Geotherm. Res. 158, 321–332.

Withers, M., Aster, R., Young, C., Beiriger, J., Harris, M., Moore, S., Trujillo, J., 1998. A comparison of select trigger algorithms for automated global seismic phase and event detection. Bull. Seism. Soc. Am. 88, 95–106.

Zobin, V., 2012. Introduction to volcanic seismology. Elsevier, Amsterdam.

Figure captions

Fig. 1 Digital elevation model of Mount Etna with location of the seismo-acoustic sensors (green triangles) and the seismic stations (blue triangles) used in this work. In the upper left inset, the digital elevation model of the summit area with the four summit craters (VOR= Voragine; BN= Bocca Nuova; NEC= North-East Crater; SEC= South-East Crater) and the position of the 13 May 2008 eruptive fissure (EF red line). The pink and orange areas indicate the dry fracture field (Bonaccorso et al., 2011) and the lava flows from the 2008–2009 eruption (Behncke et al., 2009), respectively. The position of EBEL reference station is also indicated.

Fig. 2 (a) Helicorder of infrasound signal recorded at EBEL station during 12 and 13 May 2008. **(b)** Amplitude RMS of infrasound signal recorded at EBEL station. **(c)** Time evolution of occurrence rate of infrasonic events in 30-minute-long windows.

Fig. 3 (a) Infrasonic and **(b)** vertical seismic components of two seismo-infrasonic events recorded by EBEL station, and **(c)** corresponding spectra, calculated on the signal windows comprised between the dashed vertical lines in **(a, b)**. The grey and black lines in **(c)** indicate the spectra of the infrasonic and seismic signals, respectively.

Fig. 4 Analyses of 157 infrasonic events. **(a)** Pseudospectrogram made up of 48 spectra of infrasonic events recorded at EBEL station. **(b, c)** Temporal evolution of peak frequencies calculated in the frequency bands 1-5 Hz and 0.2-1 Hz, respectively. **(d, e)** Peak-to-peak amplitudes evaluated in the frequency bands 1-5 Hz and 0.2-1 Hz, respectively.

Fig. 5 Example of infrasonic event **(a)** and the associated seismic trace **(b)** recorded at EBEL station. **(c, d)** Short Time Fourier Transform (STFT), calculated on 5.12-second-long windows, of infrasonic and seismic events, respectively. **(e)** Low-pass filtered traces (<1 Hz) of infrasound (grey) and seismic (black) signal, and the time lag between the two events.

Fig. 6 Locations of infrasonic **(a, b)** and seismic **(c-e)** events plotted with respect to time. Red dotted line indicates NEC coordinates.

Fig. 7 (a) Map of Mt. Etna with the source locations of the infrasound events, indicated by red circles. **(b, c)** Map and section of Mt. Etna with the source locations of the seismic events, indicated by red circles. The radii of the circles in **(a, b)** are proportional to the number of the locations in each grid node (see symbol legend in the lower right corner of the maps).

Fig. 8 (a) Map of Mt. Etna showing an example of the space distribution of semblance-brightness values. **(b)** Map and section of Mt. Etna showing an example of the space distribution of semblance-R^2 values. The stars indicate the grid node with the largest semblance-brightness value **(a)** and semblance-R^2 value **(b)**, respectively, for the selected seismo-acoustic event.

Fig. 9 Temporal evolution of the time lag between infrasonic traces and the associated seismic ones using cross-correlation function (orange dots) and a manual procedure (blue dots) (see text for details).

Fig. 10 (a) Photo of NEC (viewed by GoogleEarth) where the upper part of the conduit is visible at the bottom of the funnel-shaped crater. **(b)** Section showing the model of NEC conduit. Higher frequencies of infrasonic events are generated by the pipe resonance of the conduit. Further, the inferred narrowing in the upper part of the conduit makes Helmholtz resonance possible, which is responsible for the lower frequencies. All the letters reported inside the sketch indicate different physical parameters (see **equations 1, 3, 6**). **(c)** Cartoon showing a S-N section of Mt. Etna volcano with the central conduit system through which the gas-rich magma, feeding the 2008-2009 eruption, initially rose and then broke off to the east. The link between the NEC conduit and the reservoir with the gas-rich magma (located at depth of 1.6 km; Bonaccorso et al., 2011), proposed in this

work, is also reported. The dashed area and the question mark highlight the unknown depth of the link between NEC conduit and the central conduit system.

Fig. 11 Variation of theoretical frequency (visualized with the colour scale), obtained by applying the pipe resonator model (**equation 1**), as a function of conduit length and acoustic speed in the conduit. Values of the higher frequency peaks observed during the analyzed period are plotted by black contours on the graph.

Fig. 12 Variation of theoretical frequency (visualized with the colour scale), obtained by Helmholtz resonator model (**equation 3**), in relation to the conduit neck length and conduit radius.

Fig. 13 Frequency dependence of power transmission (*Tp* blue lines) and reflection (*Rp* red lines) coefficients through the narrowing, assuming a conduit radius of 25 **(a)** and 45 **(b)** m. The grey areas highlight the two frequency components characterising NEC events during the studied period. See text for details.

Fig. 14 Conduit length dependence of frequency of Helmholtz resonator frequency (f_{helm}, grey area) and of fundamental frequency ($f_{0\ pipe}$, thick black line) and harmonics ($f_{n\ pipe}$, thin black line) for closed-closed pipe resonator. In particular, the upper and the lower limits of the grey area represent the conduit length dependence of frequency of the Helmholtz resonator in the case of a 25 and 45 m conduit radius, respectively. See text for details.

Fig. 15 Variation of theoretical frequency (visualized with the colour scale), obtained by applying the Helmholtz resonator model (**equation 3**), with respect to conduit length and acoustic speed in the conduit. Values of the lower frequency peaks observed during 12 May (0.4 Hz) and before the eruption beginning on 13 May (0.7 Hz) are plotted by black contours on the graph, together with 0.3 Hz value (see text for details).

Fig. 16 Variation of theoretical time lag (visualized with the colour scale), obtained by means of **equation (6)**, in relation to source altitude, acoustic speed in the conduit and seismic velocity (*v*). Values of time lag observed during 12 May (5.4 s) and before the eruption beginning on 13 May (4.7 s) are plotted by black contours on the graph.

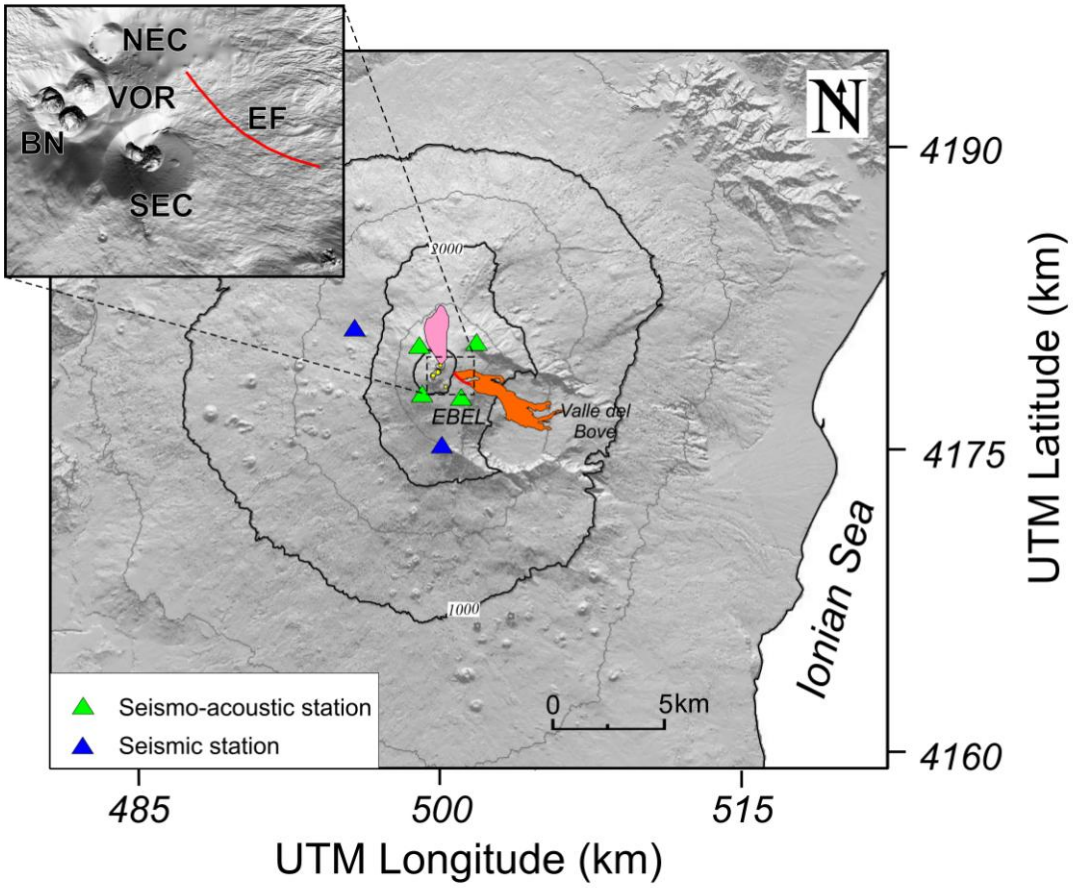

Figure 1

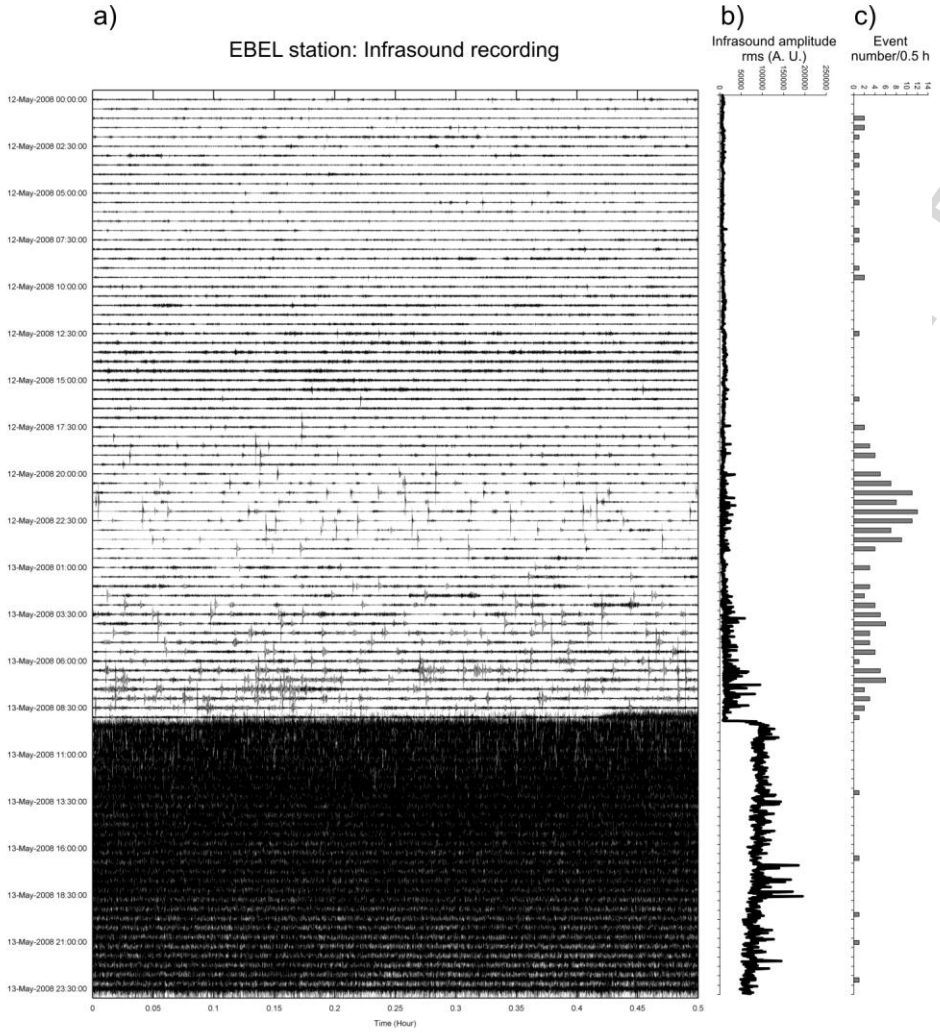

Figure 2

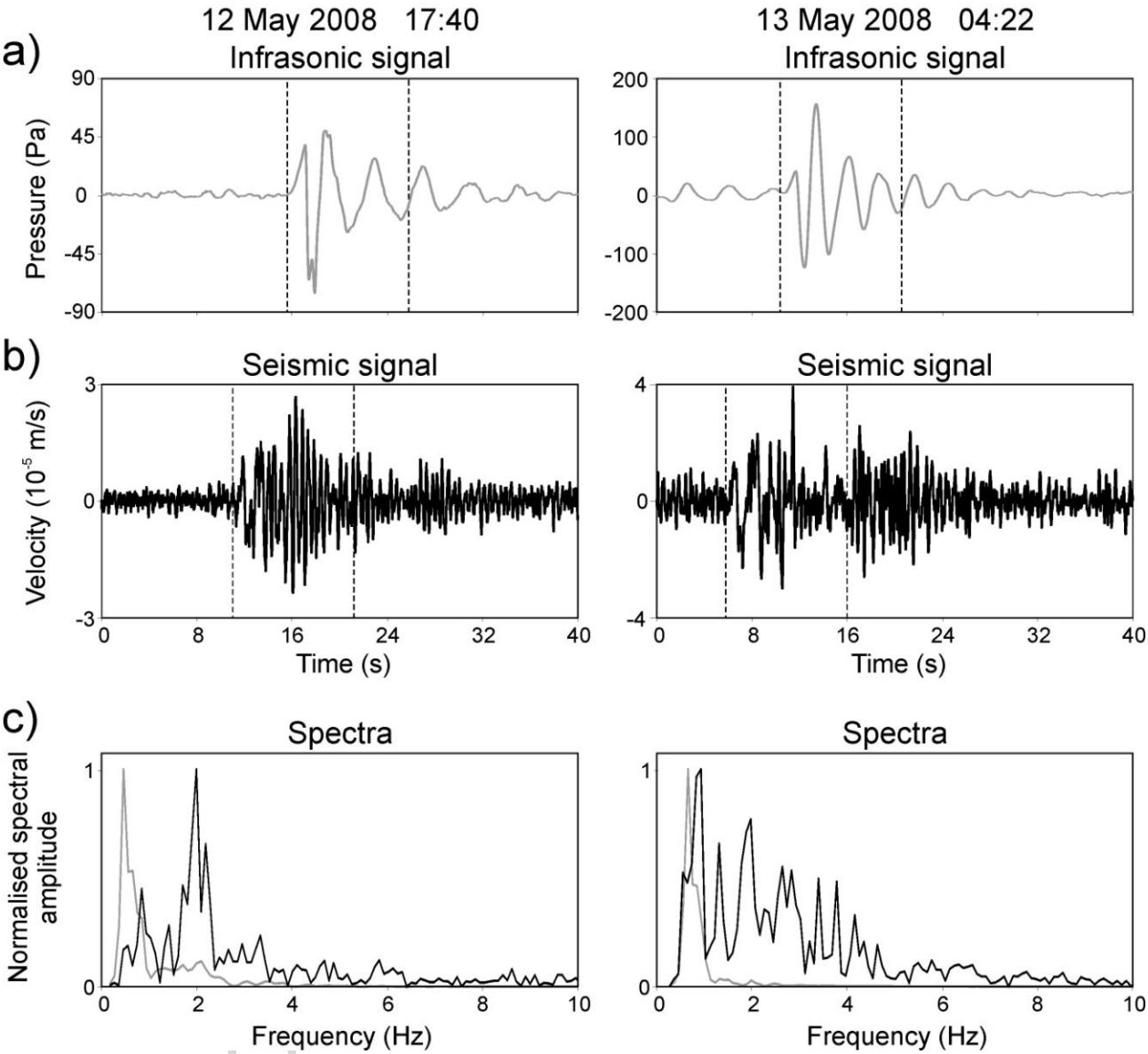

Figure 3

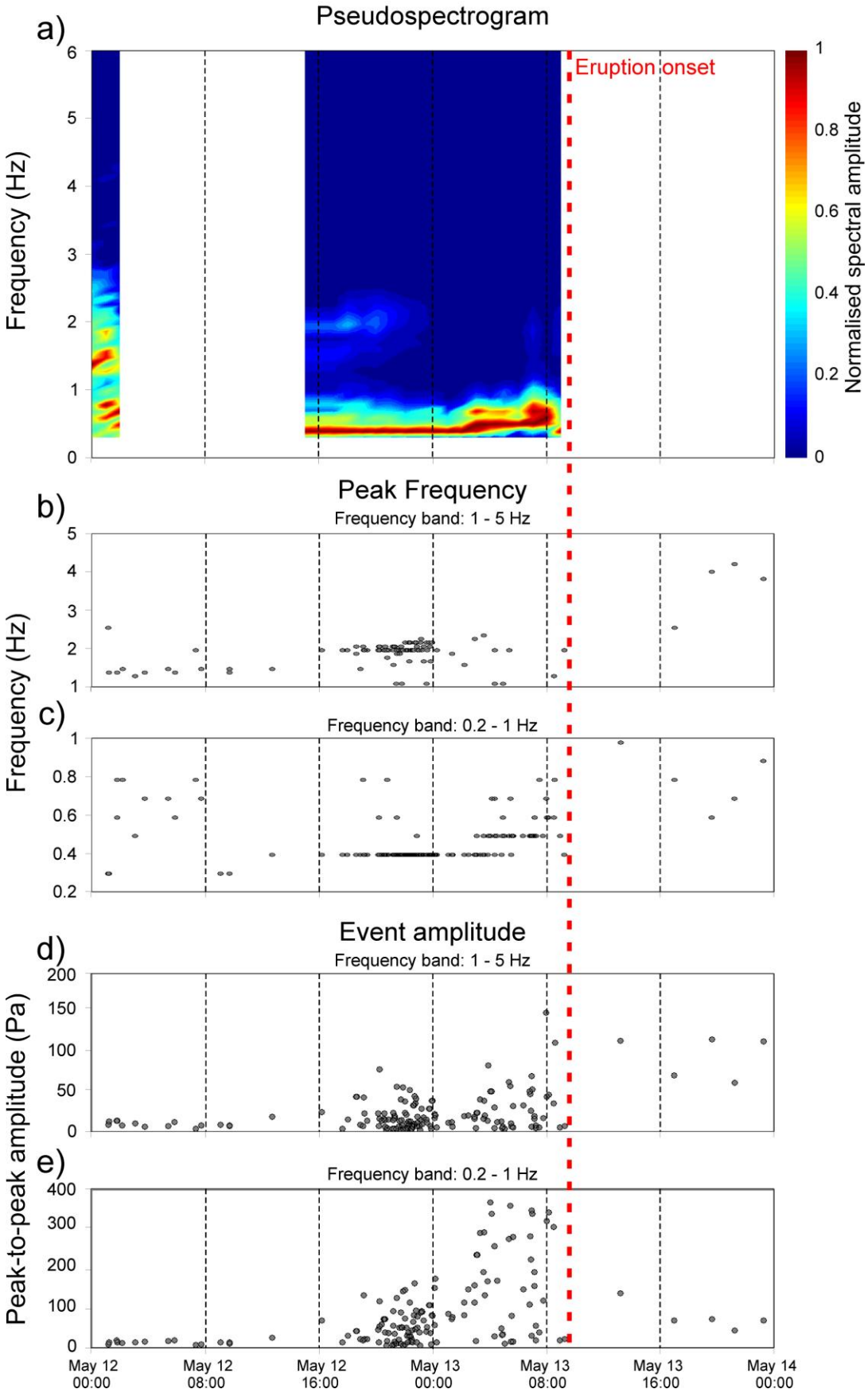
a)
Pseudospectrogram
Eruption onset
Frequency (Hz)
Normalised spectral amplitude
b)
Peak Frequency
Frequency band: 1 - 5 Hz
c)
Frequency band: 0.2 - 1 Hz
Frequency (Hz)
d)
Event amplitude
Frequency band: 1 - 5 Hz
e)
Frequency band: 0.2 - 1 Hz
Peak-to-peak amplitude (Pa)
May 12 00:00
May 12 08:00
May 12 16:00
May 13 00:00
May 13 08:00
May 13 16:00
May 14 00:00

Figure 4

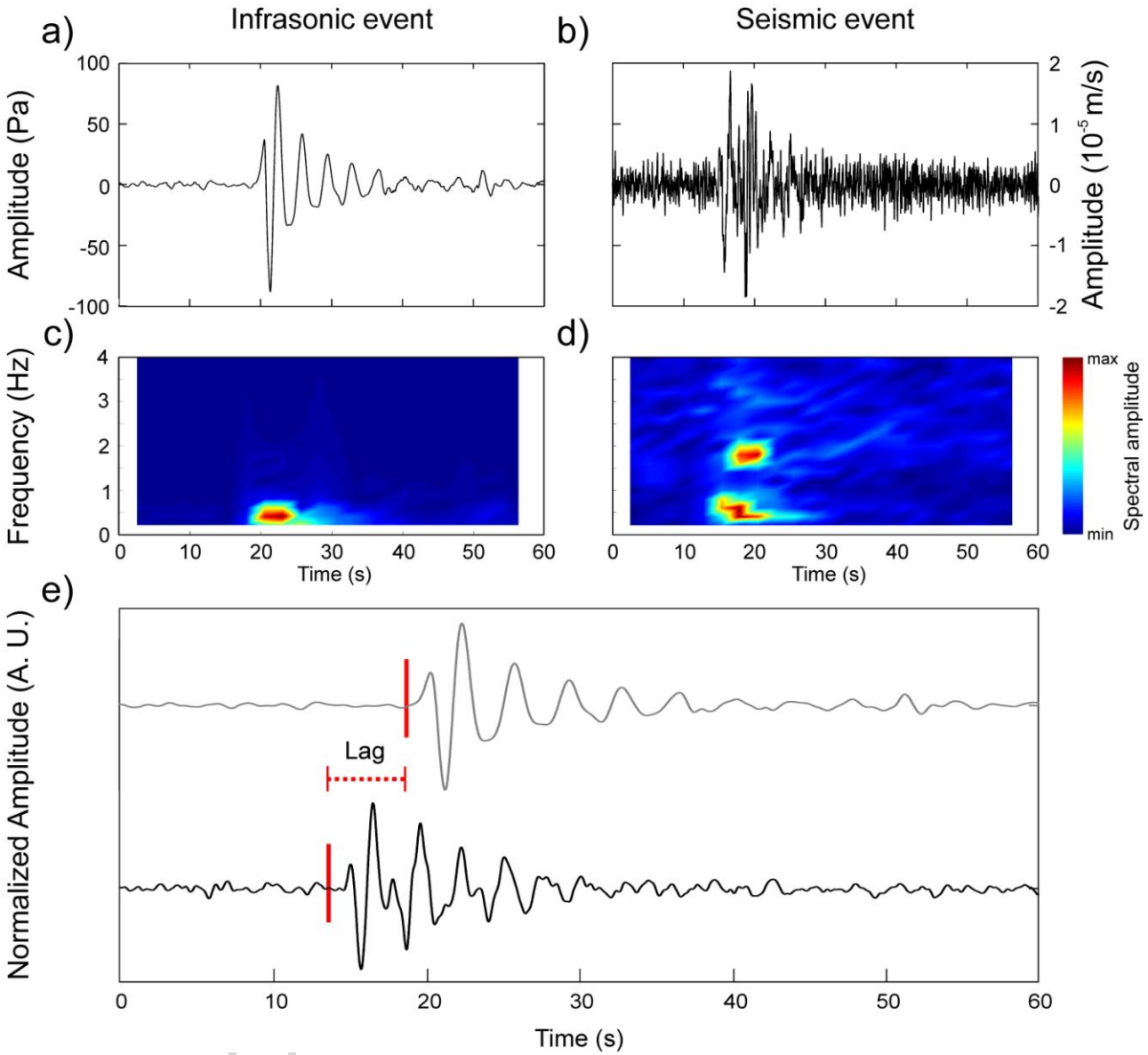

Figure 5

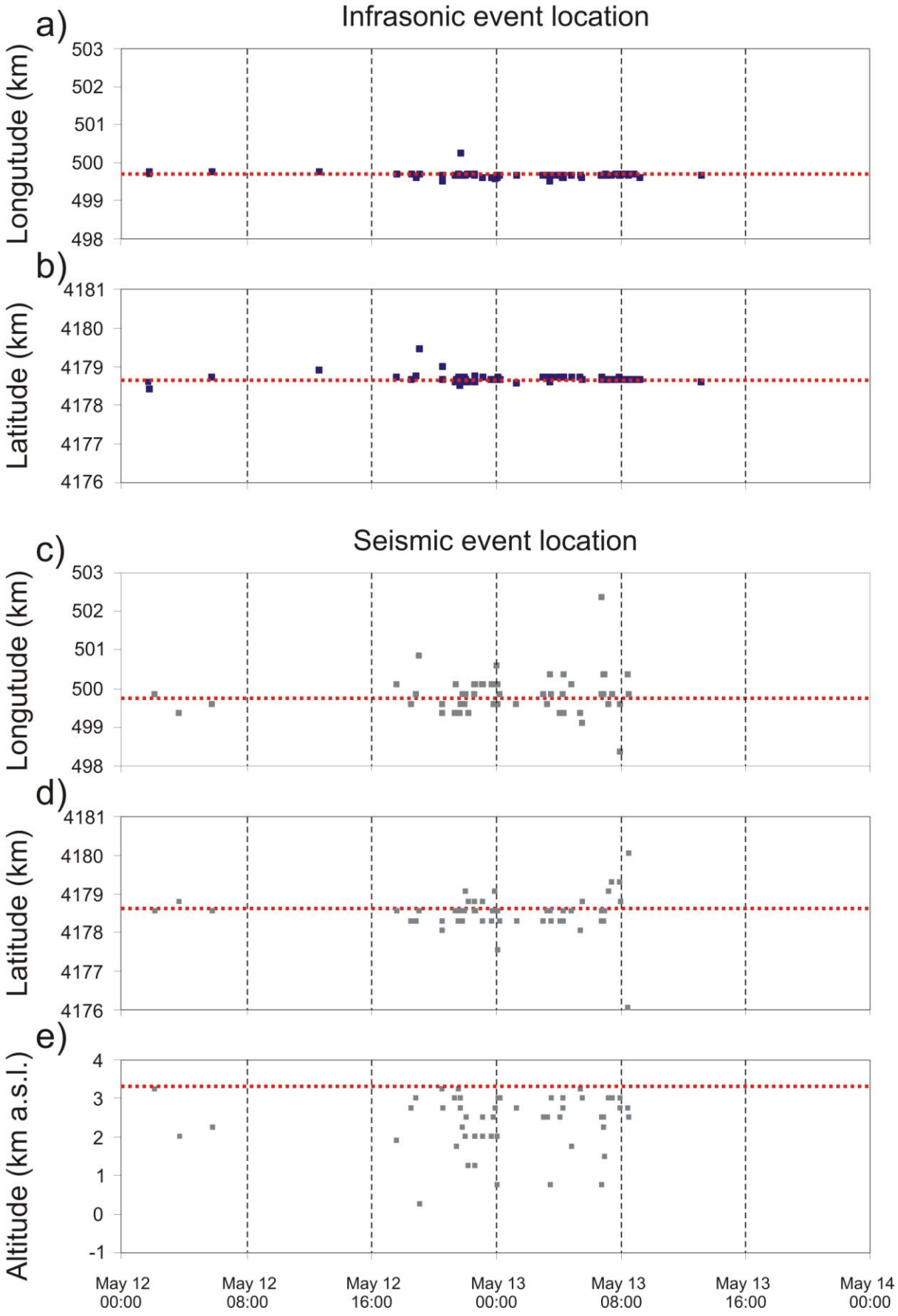
Infrasonic event location
a)
Longutude (km)
503
502
501
500
499
498
b)
Latitude (km)
4181
4180
4179
4178
4177
4176
Seismic event location
c)
Longutude (km)
503
502
501
500
499
498
d)
Latitude (km)
4181
4180
4179
4178
4177
4176
e)
Altitude (km a.s.l.)
4
3
2
1
0
-1
May 12 00:00
May 12 08:00
May 12 16:00
May 13 00:00
May 13 08:00
May 13 16:00
May 14 00:00

Figure 6

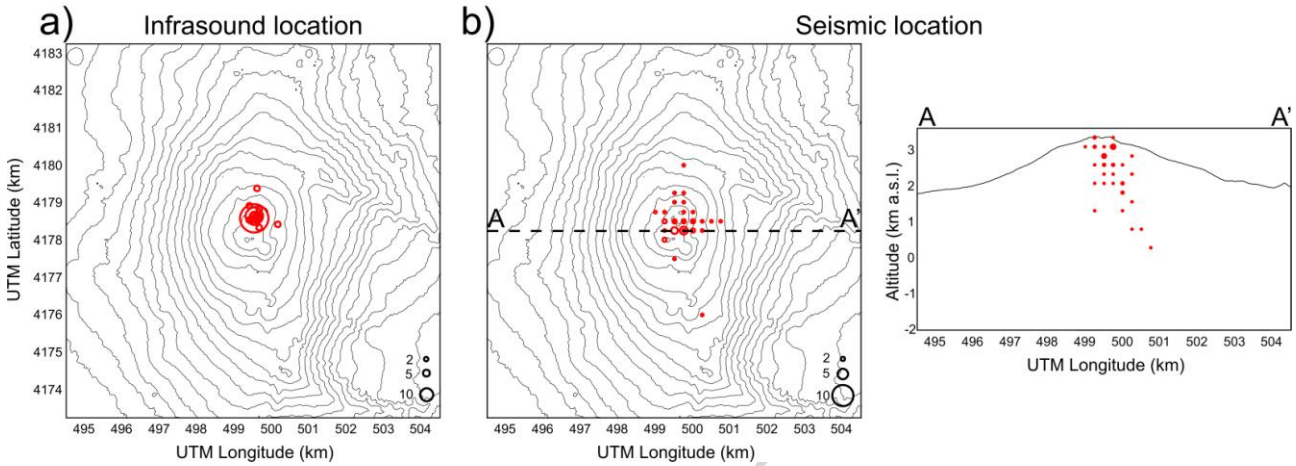

Figure 7

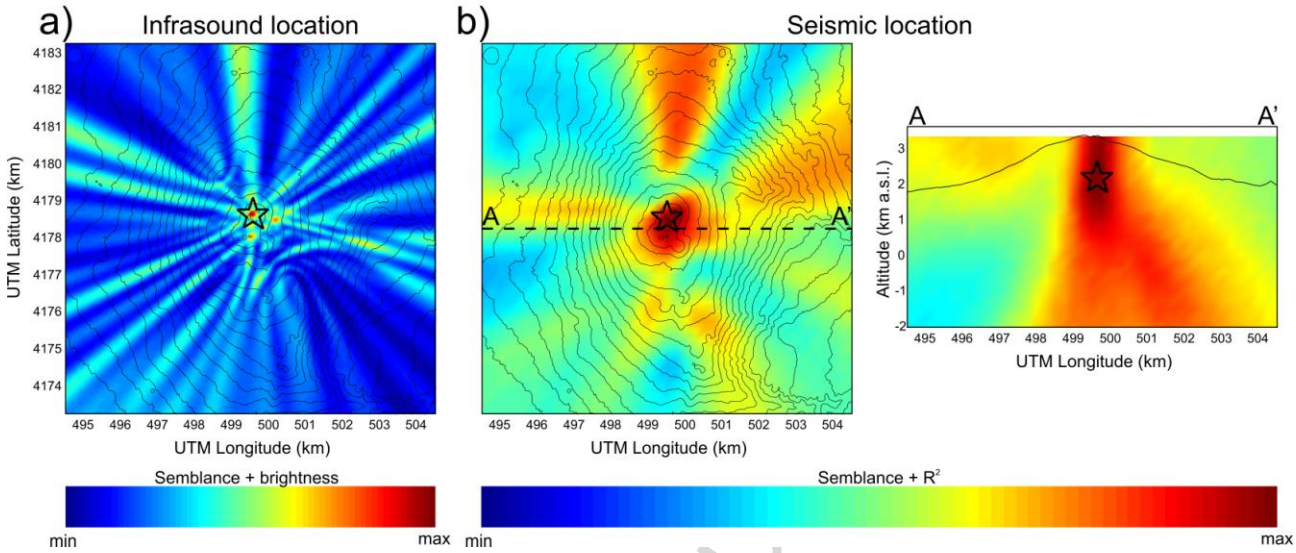

Figure 8

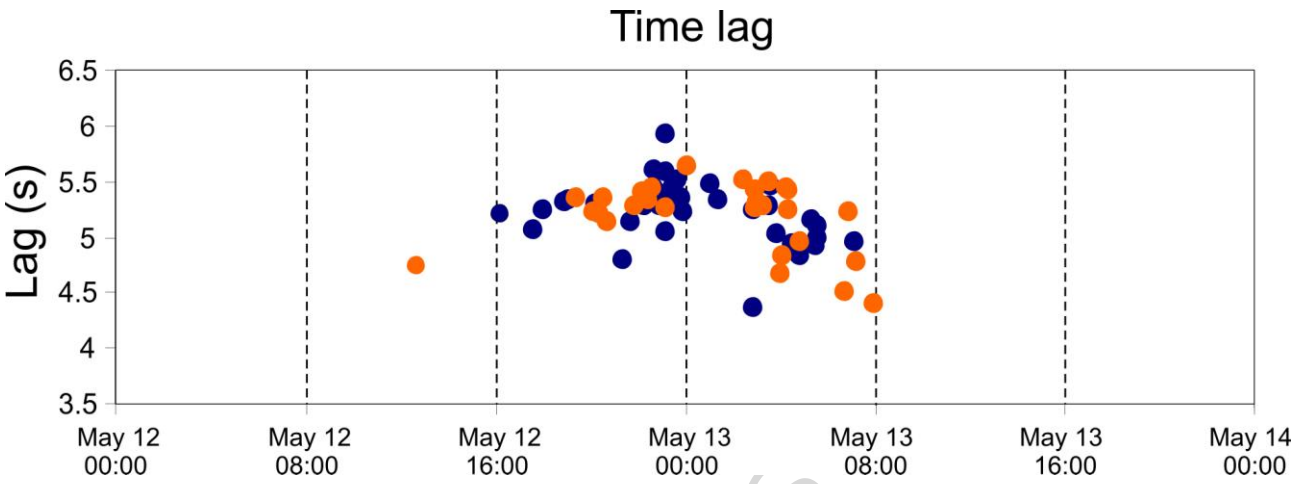

Figure 9

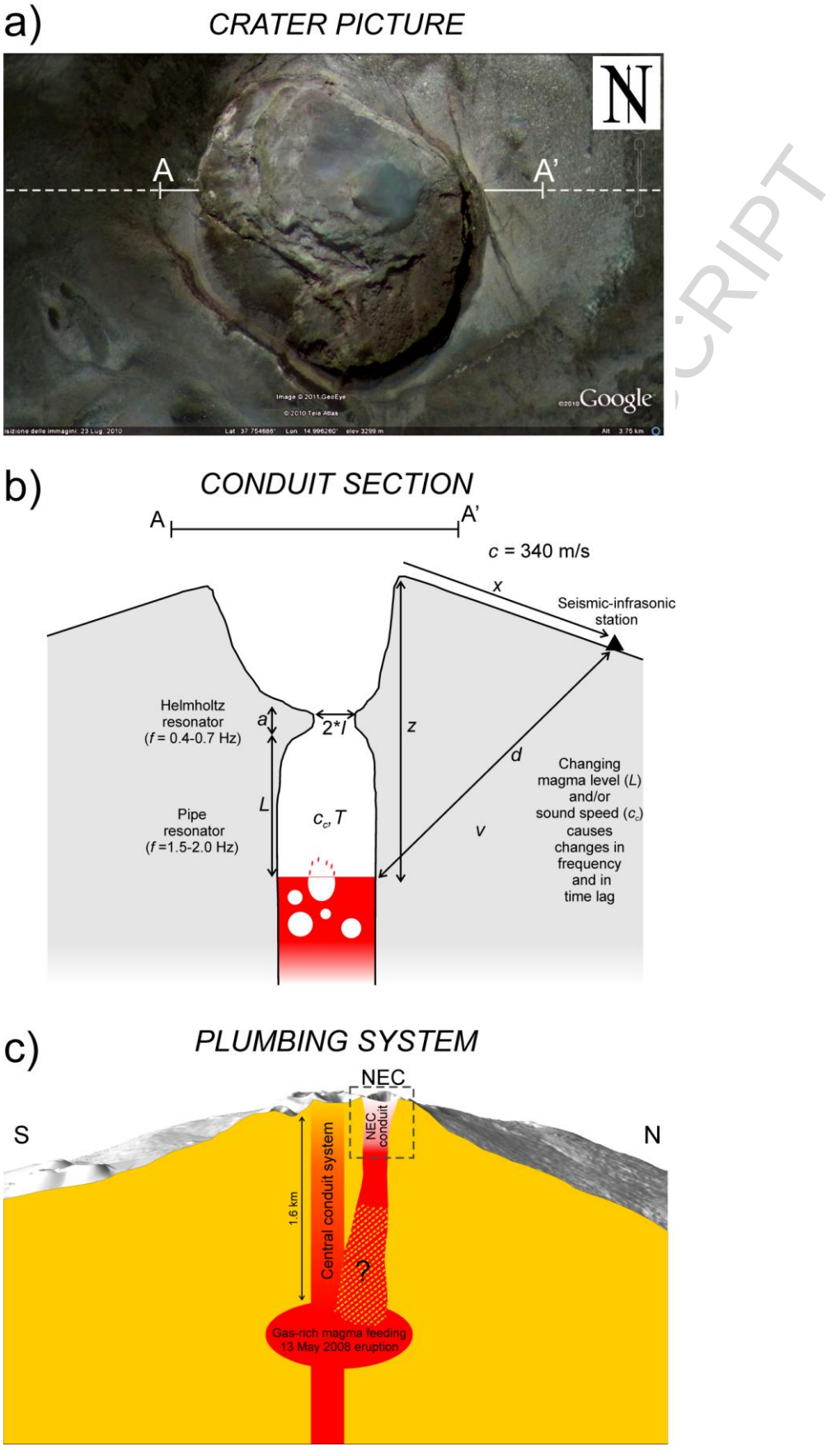

Figure 10

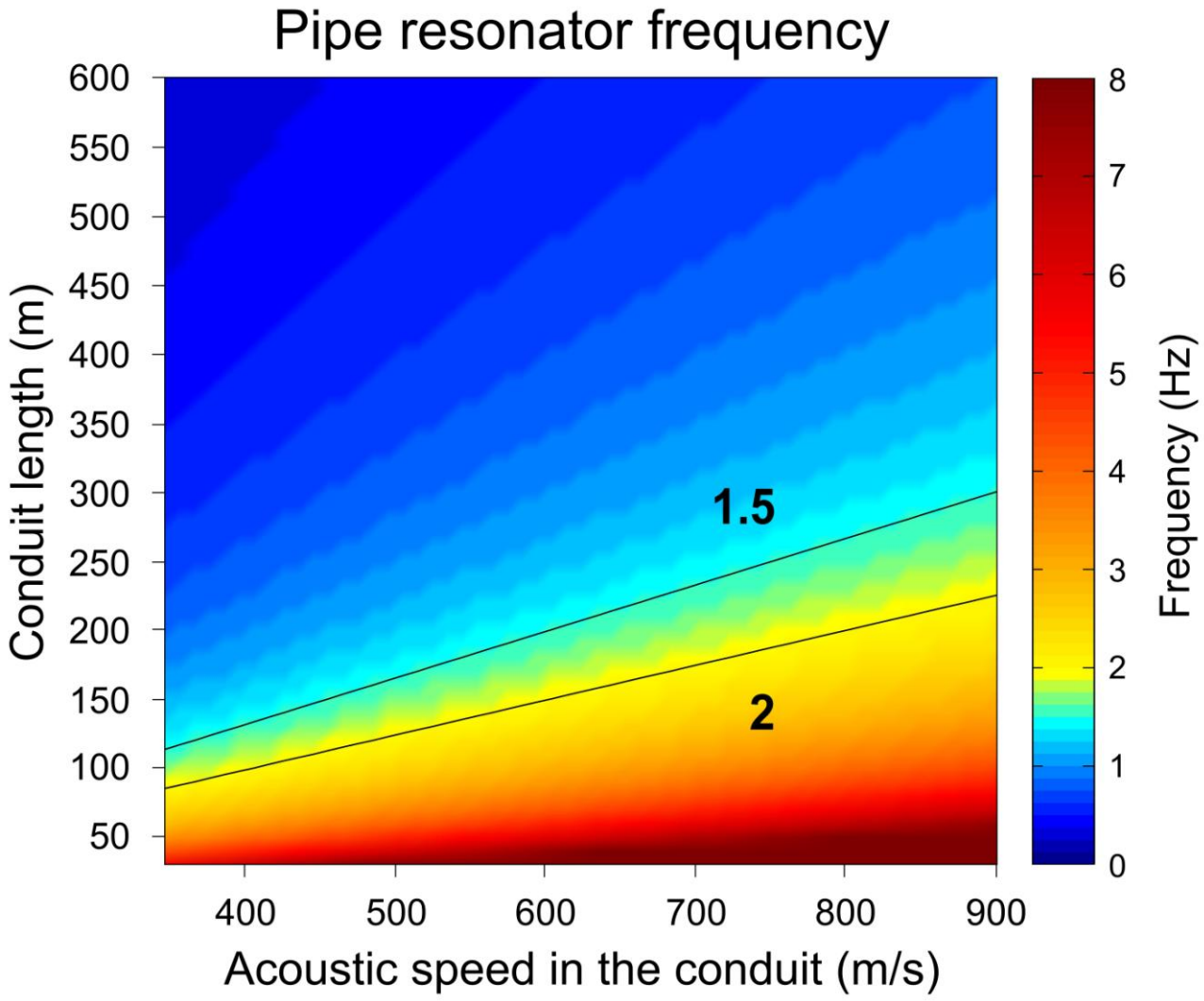

Figure 11

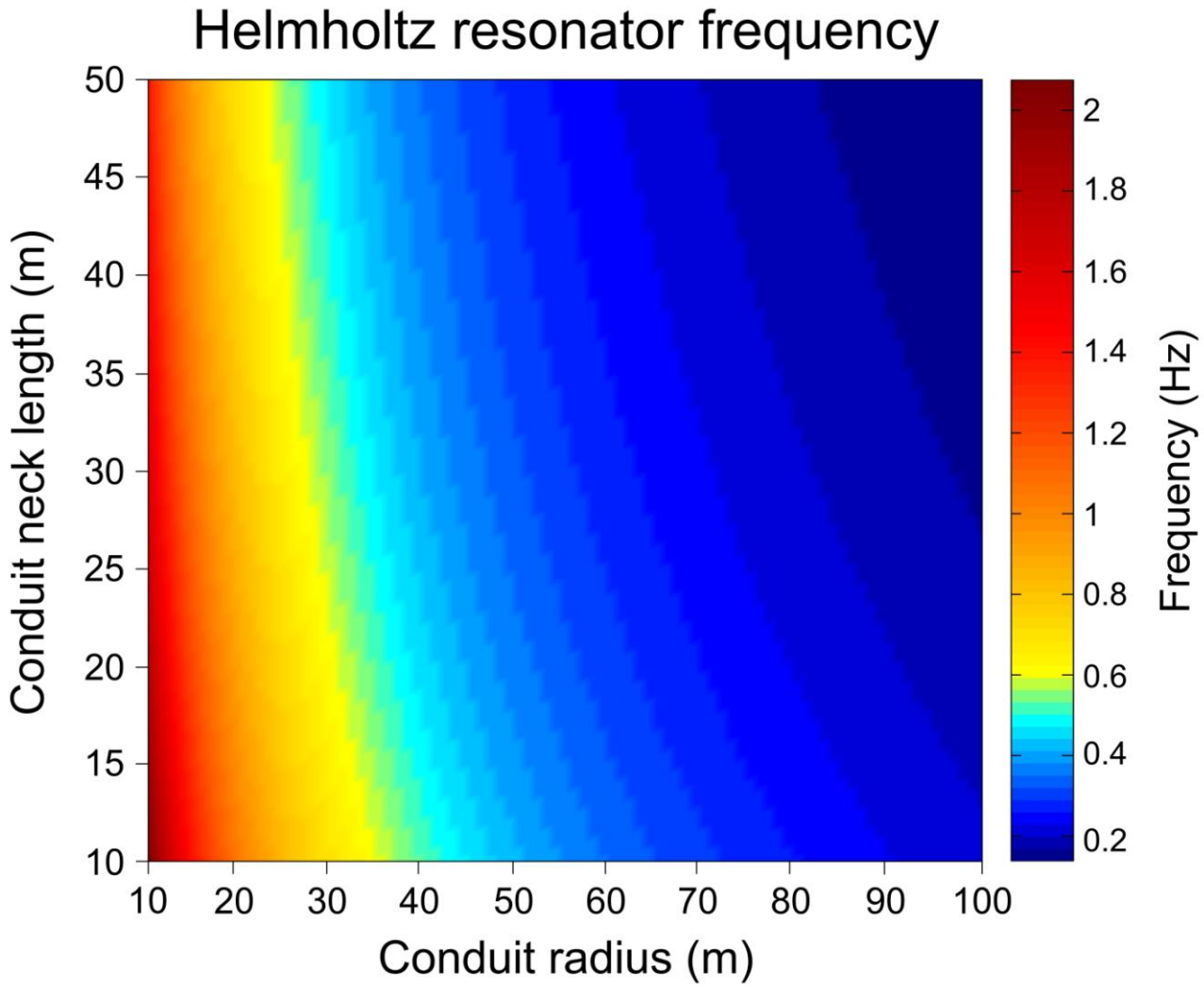

Figure 12

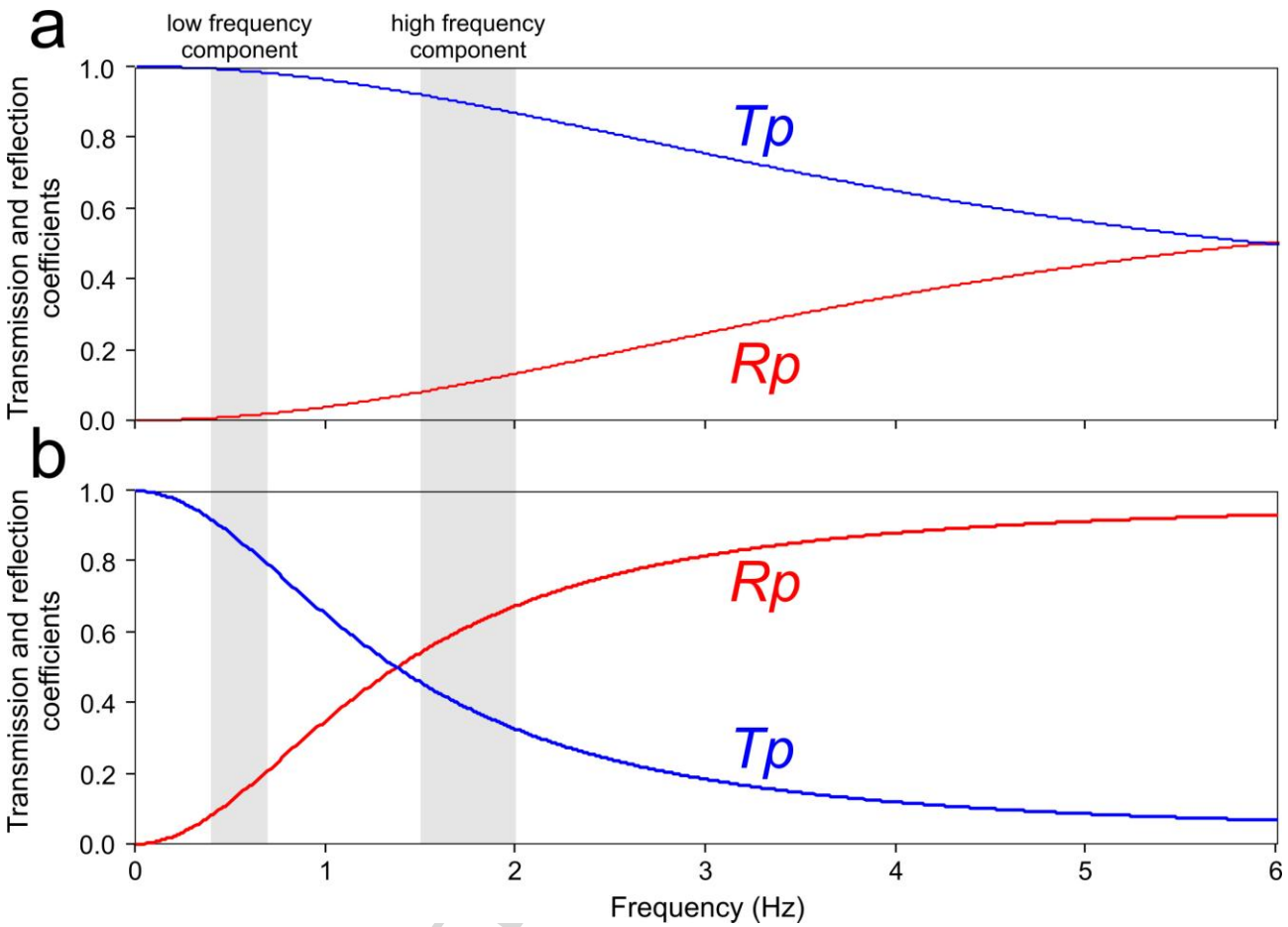

Figure 13

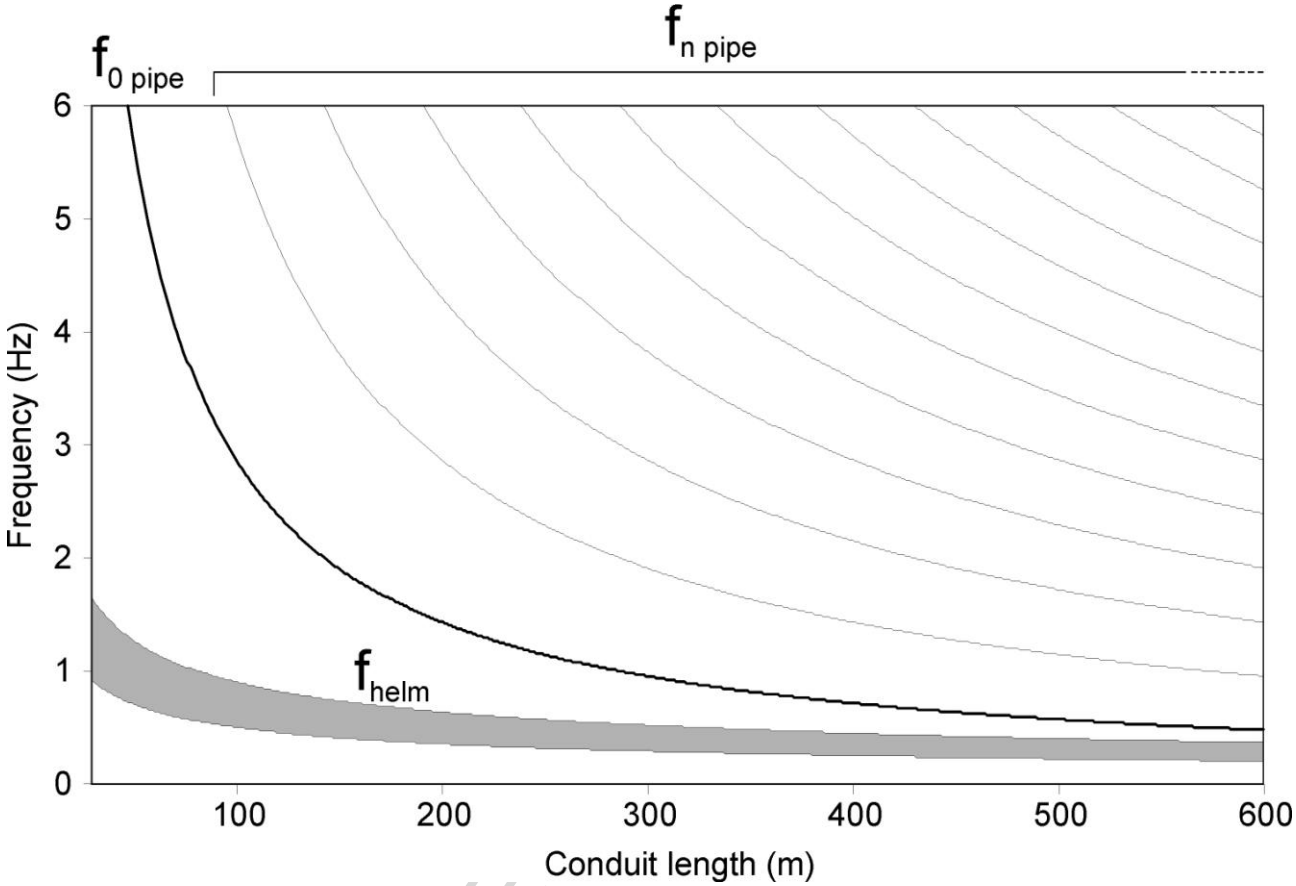

Figure 14

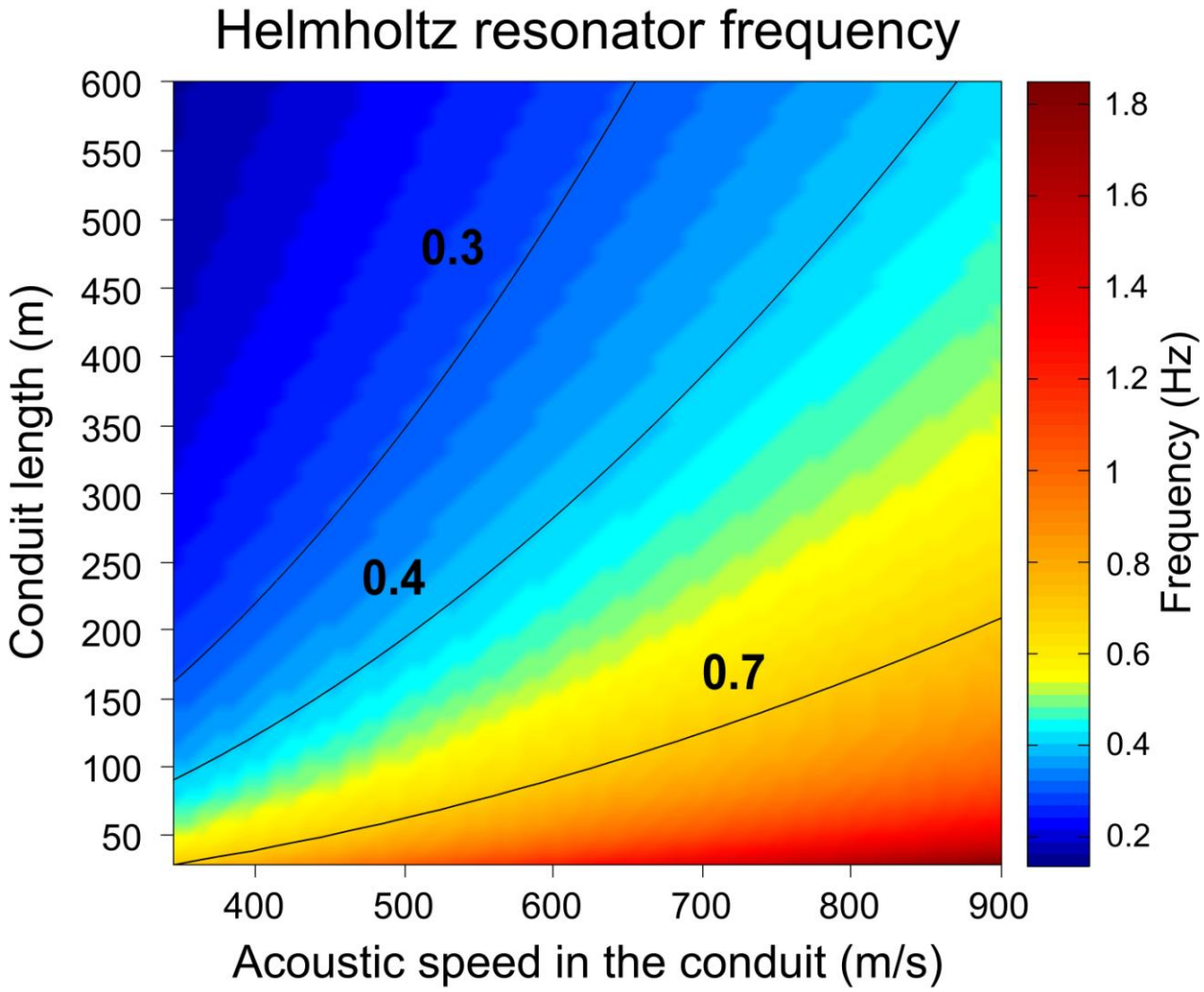

Figure 15

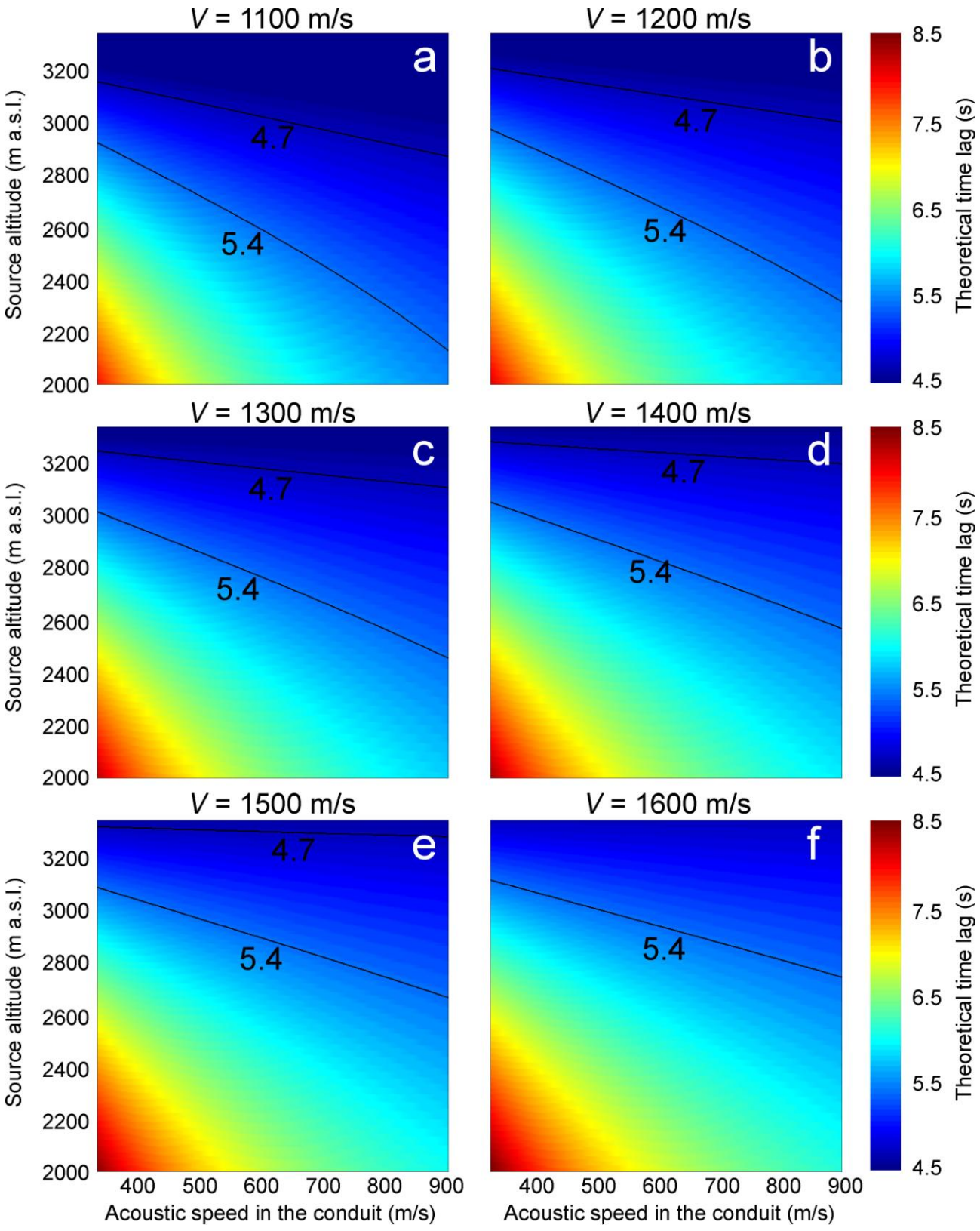

Figure 16